1-1-2010

Performance evaluation of low-cost GPS systems for static and kinematic applications

Amit Joshi
Ryerson University

PERFOMANCE EVALUATION OF LOW-COST GPS SYSTEMS FOR STATIC AND KINEMATIC APPLICATIONS

by

Amit Joshi

Bachelor of Engineering, Ryerson University

June 2007

A thesis

presented to Ryerson University

in partial fulfillment of the

requirements for the degree of

Master of Applied Science

in the Program of

Civil Engineering

Toronto, Ontario, Canada, 2010

DECLARATION

I hereby declare that I am the sole author of this thesis.

I authorize Ryerson University to lend this thesis to other institutions or individuals for the purpose of scholarly research.

Amit Joshi

I further authorize Ryerson University to reproduce this thesis by photocopying or by other means, in total or part, at the request of other institutions or individuals for the purpose of scholarly research.

Amit Joshi

ABSTRACT

Amit Joshi

PERFOMANCE EVALUATION OF LOW-COST GPS SYSTEMS FOR STATIC AND KINEMATIC APPLICATIONS

MASc., Civil Engineering, Ryerson University

2010

This thesis looks at improving positional accuracy of low-cost systems by investigating a method to isolate the multipath error based on wavelet analysis. Several sets of static and kinematic data were collected in different types of environment using a single-frequency GPS receiver. The code minus carrier combination of the GPS observables was exploited. After accounting for certain errors and resolving the ionospheric delay using ionospheric maps, the remaining terms were essentially multipath and noise. Wavelet analysis was then used to extract the multipath error. These approximations were utilized to identify and remove those satellites that were severely contaminated with multipath. Another approach investigated the subtraction of multipath approximations obtained by wavelet analysis from the corresponding code measurements. The positioning results of these two approaches were compared with those of the original data and assessed. For the static data sets, eliminating satellites contaminated with

multipath proved to be most effective. For the kinematic sessions, neither of the two approaches displayed any improvement.

ACKNOWLEDGEMENTS

I would like to thank my supervisor, Dr. Ahmed El-Rabbany for his guidance, patience, and unwavering support. I would like to thank all the other examining committee members Dr. Michael Chapman and Dr. Arnold Yuan for taking the time to read the draft.

I would like to thank my fellow friends: Hassan Ibrahim, Hamad Yousif, Mohamed El-Sobeiey, Abdulla Al-Naqbi, and Wai Yeung Yan for helping me with their sounding ideas, and answering my questions.

DEDICATION

This thesis is dedicated to my family. Without their love and support, none of this would have been possible.

TABLE OF CONTENTS

LIST OF FIGURES

LIST OF TABLES

ABBREVIATIONS

C/A	Coarse/acquisition
CWT	Continuous Wavelet Transform
DoD	Department of Defence
DOP	Dilution of Precision
DWT	Discrete Wavelet Transform
GBSS	Geodetic Base Station Software
GLONASS	Global Navigation Satellite System
GPS	Global Positioning System
HDOP	Horizontal Dilution of Precision
IGS	International GNSS Service
MRA	Multi-Resolution Analysis
NOAA	National Oceanic and Atmospheric Administration
NRCan	Natural Resources Canada
P-code	Precise
PDOP	Position Dilution of Precision
PRN	Pseudorandom Noise
RINEX	Receiver Independent Exchange
RMSE	Root Mean Square Error
SNR	Signal-to-noise Ratio
STD	Standard deviations
TEC	Total Electron Content

VDOP	Vertical Dilution of Precision
TTC	Trimble Total Control
USTEC	United States Total Electron Content

1. Introduction

The interest in utilizing low-cost GPS receivers for accurate positioning has always existed, as survey companies try to increase efficiency and reduce costs. Expensive dual-frequency GPS receivers are able to compute accurate positions usually at the millimetre-level due their ability to form linear combinations eliminating major errors through the L1 and L2 frequencies; on the other hand, low-cost systems are not as robust due to their inability to form many of the linear combinations. In general, low-cost systems are only able to track observables on the L1 frequency only. With the availability of precise products from organizations like the International GNSS Service (IGS), centimetre-level positioning can be achieved (Alkan and Saka, 2007). However the availability of precise products, such as precise ephemeris, satellite clock offsets from the IGS and ionospheric grid files from the National Oceanic and Atmospheric Administration (NOAA), have allowed major errors limiting the accuracy of single-frequency receivers to be resolved. As a result with the use of these products, accurate positioning using low-cost systems have become possible. But not all the errors are accounted for, such as multipath. A robust model to mitigate the effects of multipath still does not exist due to its environmental dependence. The purpose of this research was to evaluate the kinematic and static performances of low-cost systems in multipath environments.

1.1. Background

A literature review was conducted pertaining to the utilization of low-cost systems for precise positioning and the application of wavelet analysis for multipath mitigation. Different

types of resources were reviewed including online journals and textbooks. Below is a summary of all the relevant material.

Al-Naqbi (2008) applied wavelet analysis to determine satellites that were severely affected by multipath. GPS data from various environments were investigated. The multipath and noise were isolated by using the code minus carrier combination and resolving the ambiguity and ionospheric delay. Wavelet analysis was used to de-noise the signal and obtain an approximation for multipath. Multipath approximation values for each satellite were obtained and standard deviations were calculated. The four satellites with the smallest standard deviations were selected and positions computed. Overall, accuracies of 5 cm were achieved for baselines up to 65 km.

Alkan and Saka (2007) evaluated the use of low-cost single-frequency GPS receivers for precise positioning. Static and kinematic data were collected and processed. In the static trials, data was collected for three different occupation times: 30, 60 and 120 minutes. For the kinematic sessions, two sets of data, one lasting 12 minutes and the other 30 minutes, were gathered using a vehicle. The data was then processed using the Thales GNSS Solutions software with the implementation of precise products. Overall for the static mode, accuracies at the centimetre-level were achieved. The kinematic mode had similar centimetre-level results for the latitude and longitude. Decimetre-level accuracies were obtained for the height component.

Beran et al. (2003) developed a Kalman filter-based model for low dynamic platforms using single-frequency measurements. Three sets of static and kinematic data were collected using a low-quality single-frequency receiver and a geodetic-quality dual-frequency receiver. For the static dual-frequency data sets, the root mean square in the horizontal component produced

sub-meter accuracies, while the vertical component reached 6.8 m. On the other hand, the single-frequency receivers demonstrated meter-level results in all components. Results for the kinematic data demonstrated accuracies at the decimetre-level for the velocity components. The steady-state position components for the kinematic data resulted in accuracies in the meter range.

Ovstedal (2002) assessed different ionospheric modelling approaches for precise point positioning using single-frequency receivers. Also, the global ionospheric model produced by IGS and the Klobuchar model are evaluated. They are compared with ionospheric delay values estimated by dual-frequency observations. Precise files pertaining to the ephemeris and satellite clock corrections were implemented. The model that achieved the best results was the global ionospheric model. Overall, horizontal accuracies were below 1 m while the vertical component demonstrated accuracies of 1 m.

Elhabiby (2007) used wavelet analysis to evaluate different geodetic operators including: direct, indirect and inversion of geodetic integrals. The overall performance of wavelet in different applications is evaluated. It was determined that for different geodetic operators the wavelet thresholding technique was very effective and that wavelet compression was useful in reducing the amount of data space required for backup. Also, the de-noising of non-stationary noise can be done effectively with wavelet techniques for airborne gravimetry and satellite altimetry measurements. All in all, this dissertation demonstrated wavelet efficiencies in the evaluation of eight geodetic operators.

Zhong et al. (2008) proposed a new method of signal identification based on cross-validation. After wavelet decomposition had been performed, this method would then be used to separate noise from signals in the GPS data series. First the GPS data was separated into even

and odd series based on the indexed location of the GPS observations. The even series was utilized as the validation series; while the odd series represented the filtering series. Next, wavelet was applied to the filtering series. The approximations are then interpolated using the cubic spline function to obtain the even part of the indices for the GPS data series. The variance for the interpolated values relative to the validation series was calculated. Filtered values are extracted from the decomposed signal between the first and second subset levels. These filtered values are then regarded as another set of filtered values which are once more put through wavelet, interpolated. Various sets of data are obtained and the set with the smallest variance is taken as the signal levels of the filtering series. Wavelet coefficients are extracted and the observational series was reconstructed. Overall, improvements in GPS accuracy between 55% and 78% were obtained.

Souza et al. (2004) applied wavelet analysis to mitigate the high-frequency multipath from pseudorange and carrier phase double differences. Data was collected using a GPS receiver approximately 90 m from a building with a baseline of roughly 800 m where a permanent GPS tracking station was located. The double differenced signal was then decomposed and wavelet shrinkage was performed by thresholding, essentially removing the high-frequency multipath component from the signal. After this step, the signal was reconstructed with the high frequencies part removed. This resulted in a quicker ambiguity solution and improvements in the residuals for the pseudorange and carrier phase of approximately 30% and 24%. This paper confirmed the fact that low elevation satellites contain the greatest degree of multipath and the fact that multipath repeats itself every sidereal day.

Satirapod et al. (2001) used wavelet decomposition to separate double differenced GPS data into low- and high-frequency components. The low-frequency bias term was applied to the

GPS measurements, therefore essentially removing the bias and leaving GPS range measurements and measurement noise in the least squares process. The ambiguity resolution tests were improved and the variability in the height component was reduced by 51.8%.

Also in a more recent paper, Satirapod et al. (2005) modelled multipath using wavelet and then used the values from the model to resolve multipath in their double differenced data. GPS data were collected at two stations. One of the stations had two dual-frequency receivers connected to one antenna and was considered to have no multipath as the antenna was located on top of a building. The second station about 8 m away with another dual-frequency receiver set-up was purposely contaminated with multipath as it was placed near a concrete wall. Data was collected at a data rate of 15 seconds. Double-differenced carrier-phase residuals were obtained by using one of the receivers at the first station and another receiver at the second station. Due to the short baseline, errors like ionospheric and tropospheric delay, were ignored and what remained were multipath and observation noise. Double-differencing the zero baseline receivers resulted in the determination of observation noise. TEQC was used to calculate the multipath bias on all satellites. Next, wavelet was applied to separate the high-frequency noise with the low frequency bias for three different decomposition levels. The standard deviations of the noise from the double-differenced zero baseline receivers and approximated noise using wavelet were assessed using a statistical hypothesis test. From the data sets, an improvement of about 78% was demonstrated for the standard deviations of carrier phase after the implementation of wavelet.

Aram et al. (2007) applied wavelet analysis to approximate GPS multipath values for consumer-grade low-cost receivers. The satellites with high multipath values were eliminated and the best satellites were then used to generate position estimates. After that, the outlier positions were removed and a final improved position was obtained. 15 minute data segments

were used for seven sets of data collected over a week. To approximate multipath, an algorithm was proposed where the GPS data is passed through a db7 wavelet filters at level 5. The final positions were calculated using the best satellites for each epoch based on a set of criteria where the satellites with the highest amount of multipath were eliminated. Those values in the easting and northing directions which were beyond three standard deviations of the mean were removed and estimates for the final positions were calculated. An average improvement of approximately 60% occurred in the easting and northing variances.

Dammalage et al. (2008) used different mother wavelets and decomposition levels to approximate multipath for the C/A code. Data were collected using three GPS units set up over ground control points. One of the units was assumed to be the rover. Four sets of static data, each with the duration of 24 hours, were collected for four different multipath environments by changing the position of the reflector with respects to the rover. Multipath for the code residuals was approximated using different wavelets and decomposition levels. A comparison was then made between the calculated and extracted multipath values. It was demonstrated that the best approximation of multipath depends greatly on the mother wavelet and decomposition level selected. Overall, a 60% improvement in Differential GPS (C/A) code accuracy was achieved.

1.2. Methodology

Static and kinematic data were collected in different environments with the absence of rain and average seasonal temperatures using the Ashtech AC12 single-frequency receiver and the Trimble R7 dual-frequency receiver. The respective observation files generated by the receivers were then converted into standard RINEX format. Next, the data were manipulated,

analysed and assessed using the MATLAB computing language (MATLAB, 2009). First, the code observable was subtracted from the carrier observable leaving essentially double the ionospheric delay, the integer ambiguity term, multipath and noise. The ionospheric effects were largely removed using the ionospheric grid maps downloaded from the NOAA server. The integer ambiguity term was removed by subtracting the mean of the residual. At this stage, the remaining residual value is essentially composed of multipath and receiver noise. Wavelet analysis was then implemented to de-noise the remaining terms and to isolate the multipath error; the Daubechies wavelet, db6 (level 7) for static stations and db8 (level 9) for kinematic sessions, were specifically used. For validation, the approximated multipath values were compared with the multipath values obtained from the TEQC software (UNAVCO, 2009). After that, multipath approximation values for each epoch were subtracted with the code observable for the respective satellites in the RINEX file. Wavelet was also used to identify satellites severely contaminated with multipath. The satellites that displayed the largest standard deviations based on the wavelet approximation were eliminated for epochs with more than four satellites. Position estimates were obtained for both methods using the TTC and Bernese GPS softwares.

1.3. Objective

The overall objective of this thesis was to evaluate and assess the use of low-cost systems in both kinematic and static modes. One of the main factors hindering the application of such systems is cycle slips which result from a loss of lock on satellites. When signal loss occurs, the ambiguities are no longer fixed resulting in a jump in the phase measurements. The fixing of ambiguities is essential for precise applications. Furthermore, the presence of multipath greatly

affects positional accuracies. In order to overcome this error, wavelet analysis was introduced as a tool to enable the identification and resolution of multipath. Described below are the objectives of this research:

- Propose a new ionospheric correction approach using NOAA ionospheric grid maps;
- Develop a method to determine suitable mother wavelets and levels to be used for wavelet analysis for static and kinematic modes;
- Evaluate the implementation of multipath approximations by wavelet analysis to correct code observables;
- Examine the use of wavelet analysis to identify satellites severely contaminated with multipath; and
- Assess the quality of position estimates for single-frequency GPS data collected in different multipath environments.

2. The Global Positioning System

Throughout time, various forms of navigation have existed from dead reckoning, to compasses and maps, to the most modern form where satellites and receivers are used. Satellite based navigation is now one of the most popular ways of determining one's position. Various satellite navigation systems exist, the most popular being the Global Positioning System (GPS). In today's society, the term GPS is ubiquitous due to the popularity of vehicle navigation systems and handheld units. The practical uses and potential revenues have not only the United States GPS and Russia's GLONASS systems improving and interoperable, but will have a third system available in 2012 being European Union's Galileo (Mendizabal et al., 2009). The other nation currently planning on developing such a global system is China.

GPS is a satellite-based navigation system developed by the United States department of Defence (DoD); therefore, it is no surprise that it was initially designed for military functions. Satellites are dispersed in space around the Earth and providing a 24-hour all weather navigation service across the world.

Since GPS signals are based in the microwave region of the electromagnetic spectrum, they are therefore affected by numerous error sources including ephemeris error, satellite and receiver clock errors, antenna phase center variations, dilution of precision, receiver measurement noise, tropospheric delay, ionospheric delay and multipath. Some errors are more detrimental than others.

The ionospheric delay is one of the largest errors contaminating the GPS signal and is one of the main reasons for the signal being transmitted on multiple frequencies. However unlike

dual-frequency receivers, single-frequency units are unable to form ionospheric-free linear combinations and therefore the effects of the ionosphere need to be considered. This had led to the development of different ionospheric modelling techniques like the use of the Klobuchar model and ionospheric grid maps.

Another error that can also affect positioning accuracies is multipath. This error is difficult to model as it is environmentally dependent. The most effective method of mitigating multipath is by careful site selection. This is not always possible and therefore various hardware and software solutions are available, for example the utilization of special types of antennas, linear combinations and tools like wavelet.

2.1 Theory

The GPS system was designed to have 24 satellites equally spaced out in six different orbital planes inclined at 55 degrees to the equator. The satellites orbit the Earth's atmosphere at a height of approximately 20,180 km every 11 hours and 58 minutes passively providing its users with reliable and accurate information. Currently, there are 30 healthy satellites in orbit (Langley, 2009).

Each satellite possesses extremely precise and expensive atomic clocks. To increase their accuracy even more, the Master Control Station (MCS) pre-computes the behaviour of satellite clocks and satellite ephemerides based on data from monitoring stations across the world. This information is then uplinked to all the satellites in view and then relayed to its users travelling near the speed of light (299,729,458 m/s). In theory, all that is required to establish one's position is an accurate clock. By observing the time when the signal arrived and comparing it to

the time of transmission, it is then possible to calculate the travel time from which the distance can be determined.

(Distance) = (Travel Time) * (Speed of Light)

In order for the user to calculate its position, a minimum of four distances are required accounting for: horizontal positions, vertical position and timing error. By knowing the position of the satellites and their respective distances to the receiver, one can then solve for the receiver position.

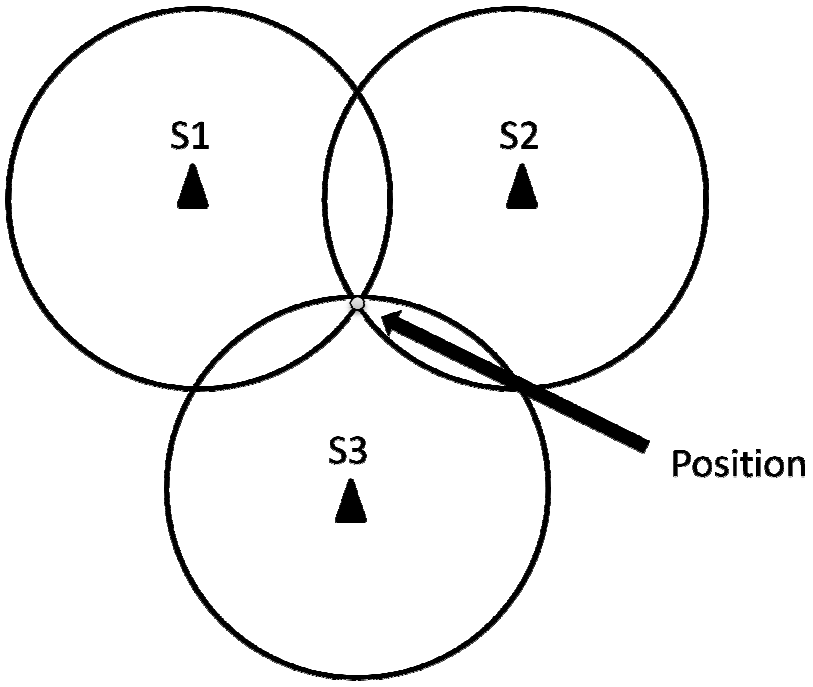

Figure 2.1 Concept of GPS based on three satellites

Two carrier waves, L1 and L2, are transmitted by all GPS satellites. The L1 and L2 frequencies are 1575.42 MHz and 1227.60 MHz, respectively. Two pseudorandom noise (PRN) codes are modulated on these frequencies, being the Coarse/Acquisition (C/A) code and Precise

(P) Code. These pseudorandom noises are generated by a special algorithm known as Tapped Feedback Shift Registers.

Two new civil codes on L2, L2 civil-long (L2 CL) code and L2 civil-moderate (L2 CM) code, and two new military (M) codes will be added on both frequencies in accordance with the modernization plan (El-Rabbany, 2006). The M-code was first broadcasted on September 25, 2005 (Lachapelle and Petovello, 2006). Also in accordance with this plan, a new carrier will be added called L5C with a frequency of 1176.45 MHz which will attain initial operational capability between 2010 and 2020 (Sickle, 2008).

2.2 Observables

To determine one's position, two types of GPS observables are used. Each observable is associated with a different resolution. Where precision is not extremely relevant, such as applications in navigation, the code pseudorange is sufficient. However, in instances like surveying where high precision is required, the phase pseudorange needs to be exploited.

2.2.1. Code Pseudorange

The distance measured between the user and a satellite is known as the pseudorange. The term pseudorange is applied due to errors in time measurements caused by cheap crystal clocks in the GPS receiver. When the GPS receiver is turned on, it knows exactly where the satellites are and can replicate the C/A-code signal. When the satellite signal is received, the code in the receiver will not match up perfectly with the one received from the satellite. Differencing both

times will yield the signal travel time. This difference multiplied by the speed of light, is used to compute the distance between the satellite and the receiver. The C/A- and P-code have a resolution of 300 m and 30 m respectively. The code pseudorange can be depicted as:

$$P_i^j(t) = \rho_i^j(t, t-\tau) + c\left[dt_i(t) - dt^j(t-\tau)\right] + c\left[d_i(t) - d^j(t-\tau)\right] + d_{trop}^j + d_{ion}^j + d_{mp}^j + \epsilon_p^j \quad (2.1)$$

Where,

P	is the measured code pseudorange (m)
ρ	is the geometric distance between the antennas of satellite j and receiver i (m)
c	is the speed of light (299,729,458 m/s in vacuum)
t	is the GPS time (s)
τ	is the signal travel time (s)
$dt_i(t)$	is the receiver clock error with respect to GPS time (s)
$dt^j(t-\tau)$	is the satellite clock error with respect to GPS time (s)
$d_i(t)$	is the code receiver hardware delay (s)
$d^j(t-\tau)$	is the code satellite hardware delay (s)
d_{trop}^j	is the tropospheric delay (m)
d_{ion}^j	is the ionospheric delay (m)
d_{mp}^j	is the code multipath error (m)
ϵ_p^j	is the code receiver noise (m)

2.2.2. Phase Pseudorange

Another type of range is known as the phase pseudorange. The resolution of phase is a lot finer, with a wavelength of roughly 19 cm and 24 cm respectively for the L1 and L2 frequencies. The dilemma with the phase is that the receiver is unable to distinguish between full carrier cycles.

Once the receiver obtains a lock on a satellite, it is able to measure the initial fraction of a cycle but not the full sinusoidal cycles. The unknown number of cycles is known as the ambiguity term. This term does not change unless the lock on satellites is lost. Correct resolution of the integer ambiguity parameter is extremely important when trying to achieve high positional accuracy. The phase pseudorange can be described as:

$$\Phi_i^j(t) = \rho_i^j(t, t-\tau) + c\left[dt_i(t) - dt^j(t-\tau)\right] + c\left[\delta_i(t) - \delta^j(t-\tau)\right] + \lambda\left[\Phi_i(t_o) - \Phi^j(t_o)\right] + \lambda N + d_{trop}^j - d_{ion}^j + \delta_{mp}^j + \epsilon_\Phi^j \quad (2.2)$$

Where,

Φ	is the measured phase pseudorange (m)
$\Phi_i(t_o)$	is the non-zero initial phase of the receiver (cycles)
$\Phi^j(t_o)$	is the non-zero initial phase of the satellite (cycles)
λ	is the carrier wavelength (m)
N	is the integer cycle ambiguity (cycles)
$\delta_i(t)$	is the phase receiver hardware delay (s)
$\delta^j(t-\tau)$	is the phase satellite hardware delay (s)
δ_{mp}^j	is the phase multipath error (m)
ϵ_Φ^j	is the phase receiver noise (m).

2.2.3. Code Minus Carrier Combination

A MATLAB algorithm was created to extract the code and phase observables from the respective RINEX file and then to compute their differences. The code pseudorange can be subtracted from the carrier pseudorange resulting in Equation 2.3:

$$P_i^j(t) - \Phi_i^j(t) \cong \; c\left[d_i(t) - d^j(t-\tau)\right] + 2d_{ion}^j + d_{mp}^j + \epsilon_p^j - \lambda N - \lambda\left[\Phi_i(t_o) - \Phi^j(t_o)\right] - c\left[\delta_i(t) - \delta^j(t-\tau)\right] - \delta_{mp}^j - \epsilon_\Phi^j \quad (2.3)$$

Due to the subtraction of both observables, the tropospheric delay, clock errors, antenna phase centre variations, relativistic and geometry effects were removed. The remaining terms are: multipath error on the code and carrier, double the ionospheric delay, the hardware delays, the receiver noise and the ambiguity.

$$P_i^j(t) - \Phi_i^j(t) \cong c\left[d_i(t) - d^j(t-\tau)\right] + 2d_{ion}^j + d_{mp}^j + \epsilon_p^j - \lambda N - \lambda\left[\Phi_i(t_o) - \Phi^j(t_o)\right] - c\left[\delta_i(t) - \delta^j(t-\tau)\right] \quad (2.4)$$

The negligible terms in the above equations are the multipath and noise on the carrier phase, as these values are minute when compared to the code reducing Equation 2.3 to Equation 2.4. Since the differential hardware delay is stable over time, it can be removed by taking the mean of the residual (El-Rabbany, 2006). The integer cycle ambiguity and the effects of the initial phases can also be removed because it is considered to be stable over time as the receiver is able to track changes in the phase as long as cycle slips are not present in the data.

$$P_i^j(t) - \Phi_i^j(t) \cong 2d_{ion}^j + d_{mp}^j + \epsilon_p^j \quad (2.5)$$

Equation 2.5 depicts the remaining values of two times the ionospheric delay, multipath and noise. The ionospheric delay parameter was removed by calculating the amount delay using TEC files downloaded from the NOAA website described in Section 3.1.4. At this stage, we are essentially left with low-frequency multipath and high-frequency noise (Fu et al., 1997) demonstrated by Equation 2.6.

$$P_i^j(t) - \Phi_i^j(t) \cong d_{mp}^j + \epsilon_p^j \tag{2.6}$$

Figure 2.2 demonstrates the effects of resolving the ionospheric delay from values obtained from the NOAA website.

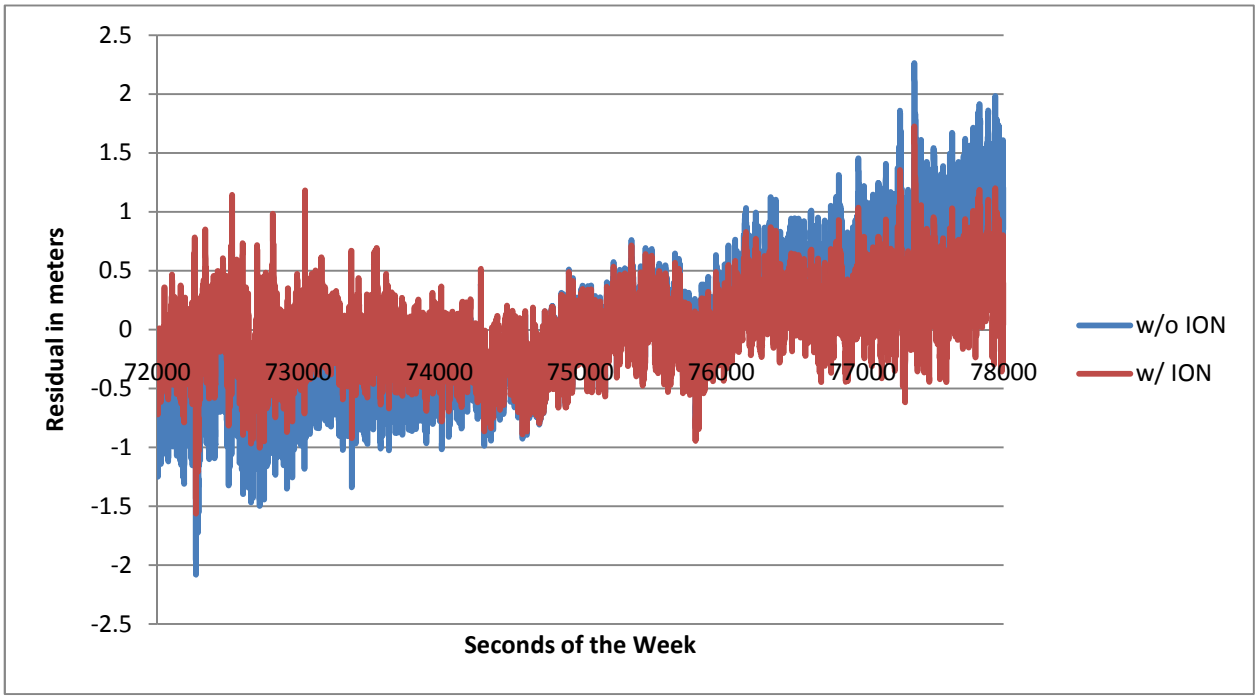

Figure 2.2 Comparison between the residuals with and without the USTEC ionospheric correction (ION)

2.3. Error Sources

As indicated above, there are a number of errors and biases degrading positional accuracies. These errors are often categorized into four sections with errors stemming from the satellite, receiver, along the signal propagation path, and geometric effects.

- **Ephemeris Errors**

  Ephemeris error results from the differences in the actual and expected satellite position due to modeling inaccuracies determined by the Master Control Station. Four-hour GPS data spans are used to predict satellite positions for a one-hour period. These predictions can lead to errors normally in the meter range for the broadcast ephemeris (El-Rabbany, 2006).

  In order to increase positional accuracies, precise ephemeris files should be exploited. These files can be downloaded from the IGS website. Precise ephemeris files are accurate to approximately 2.5 cm (IGS, 2009). Furthermore, this error can be significantly diminished by the employment of between-receiver single difference and double-differenced observable for relatively short baselines, generally up to a few tens of kilometres (Sickle, 2008).

- **Selective Availability**

  Selective Availability (SA) was initiated on March 25, 1990, for national security reasons. The intentional degradation of the GPS signal was accomplished by dithering the satellite clock frequency and providing only a coarse description of the satellite ephemeris, resulting in incorrect satellite positions. Therefore, only authorized users would reap the true potential of autonomous GPS positional accuracies while typical civil users could experience horizontal and vertical errors up to 100 and 156 m at a 95% probability level. On May 1, 2000, SA was officially turned off allowing all types of GPS users to obtain better positional accuracies (El-Rabbany, 2006).

- **Satellite and Receiver Clock Errors**

  Atomic clocks aboard GPS satellites are generally composed of rubidium or cesium materials, which are extremely precise but not perfect. The imperfections accompanying atomic clocks on board GPS satellites translate into positional errors affecting all of the C/A-code and P-code users equally, independent of satellite direction. These clocks typically stray approximately 8.64 to 17.28 nanoseconds per day translating into 2.59 to 5.18 meters (El-Rabbany, 2006). A large part of the satellite clock error can be removed by extracting the satellite clock information in the broadcast navigation message and applying them to a polynomial equation. On the other hand, receiver clocks are made out of inexpensive crystal clocks making them relatively inaccurate. A method of accounting for the receiver clock error is by between-satellite differencing.

- **Dilution of Precision**

  The geometry of satellites locked onto a particular GPS receiver will have an affect on the positional accuracies obtained by the user. The measure of instantaneous satellite geometry is known as Dilution of Precision (DOP). The best positional accuracy when four satellites are in view is achieved when three satellites are equally spaced at the minimum elevation angle around the horizon and one satellite is directly overhead (Spilker and Parkinson, 1996). A good satellite configuration will result in a small DOP value. Conversely, satellites clustered together will produce a greater DOP value due to a larger area of uncertainty. DOP can be broken down into several components: Position Dilution of Precision (PDOP) which relates to the three dimensional coordinates, Horizontal Dilution of Precision (HDOP), Vertical Dilution of Precision (VDOP) and Time Dilution of Precision (TDOP).

- **Multipath**

  Multipath occurs when a signal arrives at an antenna through more than one path. The GPS signal reflects off of surrounding objects like buildings and trees causing errors in the pseudoranges and carrier phase. This error is environmentally dependent; therefore, careful site selection is important when trying to reduce multipath.

- **Receiver Measurement Noise**

  Random measurement noise, called receiver noise, is due to limitations in the receiver's electronic. This error affects both the code and carrier measurements as they cannot be

measured perfectly and are subject to random influences. In general, the noise in a signal is about 1% of the signal wavelength (Seeber, 2003). For example, the wavelength on L1 carrier phase is approximately 19 cm; therefore, about 1.9 mm of noise is expected. Over the years, advances in GPS receiver technology have lead to a reduction in receiver noise where internal phase noise is expected to be below 1 mm and the code to be at the 10 cm level (Seeber, 2003).

- **Antenna Phase Center Variations**

  Errors in the phase center variations for both the satellite and ground station antennas are among one of the sources hindering the effectiveness of high precision GPS positioning. This is caused by the difference between the electrical phase center of the antenna and geometrical center of the antenna. Calibrations for antenna phase center variations are used to increase precision for applications such as engineering surveys, where accuracies at the millimetre-level are required.

- **Tropospheric Delay**

  Any GPS signal propagating through the lowermost part of the Earth's atmosphere will be refracted; therefore, the electromagnetic path taken by the GPS signal will be longer than its geometric path. The increase in length will augment the time travelled by the signal to reach the receiver. This time difference delays the GPS signal causing errors in position. The resulting bias is a function of the atmospheric temperature, pressure and moisture content. This delay occurs in the tropospheric and stratospheric layers of the

atmosphere and is referred to as tropospheric delay or tropospheric propagation delay, due to the bulk of delay occurring in the troposphere (Mendes, 1999). Also, the region in which the delay occurs is frequency independent and is, therefore, non-dispersive for GPS signals and other radio waves up to 15 GHz (El-Rabbany, 2006).

A plethora of empirical models, most notably the Hopfield model and Saastamoinen model, try to correct for the tropospheric delay. First, the delay is modeled at the zenith and then projected by mapping functions to the desired line of sight. The delay can be broken down into dry and wet components. The dry part accounts for approximately 90% of the total tropospheric delay, while roughly 10% is due to the wet component. Most models are very good at accurately predicting the dry component of the tropospheric delay, but not the wet component it depends on the amount of water vapour that the signal passes through (Mendes, 1999).

- **Ionospheric Delay**

The GPS signal is bent and changes speed when it passes through the ionospheric layer of the Earth's atmosphere causing positional errors. This distortion was initially one of the main reasons for using dual-frequency receivers where through linear combinations, this error could largely be removed. The magnitude of the ionospheric delay varies with geographic location, time of the day, season of the year, magnetic activity, and the direction of observation (Seeber, 2003).

3. Ionospheric and Multipath Effects on GPS Signal

In order for the GPS signal to reach the user, it has to travel approximately 20000 km from space. Along the signal path, it is affected by different types of perturbing forces which have different degrees of impact on the estimated pseudoranges. The signal first passes through the ionosphere where the electron density of the atmospheric layer causes delays in the signal. After that, the signal reaches the stratosphere and troposphere where again the signal is delayed, however this time, it is mainly due to the dryness of this region of the atmosphere. When reaching the Earth's surface, the direct path of the signal may be obstructed by surrounding objects, therefore causing the signal to be bent reflected or blocked. This will obviously cause additional errors to the pseudoranges. This chapter will focus mainly on the ionospheric delay and multipath.

3.1. Ionospheric Effect

Gases surrounding the Earth are stratified and referred to as the atmosphere. The region between approximately 50 km and 1000 km above the Earth's surface, where electrons and ions roam freely, is known as the ionosphere. The radiation emitted from the sun interacts with gas molecules causing them to ionize. The presence of charged particles causes this region in the atmosphere to behave like an electric conductor affecting passing radio waves. If not accounted for, the ionospheric effects on GPS positional accuracy can be quite detrimental (Hofmann-Wellenhof et al., 2008).

3.1.1. Ionospheric Layers

The ionosphere is divided into four layers: D, E, F and topside. Each layer contains a certain degree of ionization and its area can vary during the day due to insulation of the Sun (Seeber, 2003). Between 50 and 90 km above the Earth lies the D-layer where mainly the weak ionization occurs, and is responsible for the absorption of radio waves with high frequencies. This layer is only active on the daylight side of the Earth (Seeber, 2003). Just above is the E-layer, located between 90 and 150 km above the Earth's surface. After this follows the F-layer which lies above 150 km to about 600 km above Earth's surface. The F-layer can be further divided into F_1- and F_2-layers. The F_2-layer is where the concentrations of electrons are the highest. The last layer, the topside, begins at a height of the maximum density of the F_2-layer. The ionosphere extends to approximately 1000 km; however, no real boundary exists between the ionosphere and the Earth's magnetic field (Anderson and Fuller-Rowell, 1999).

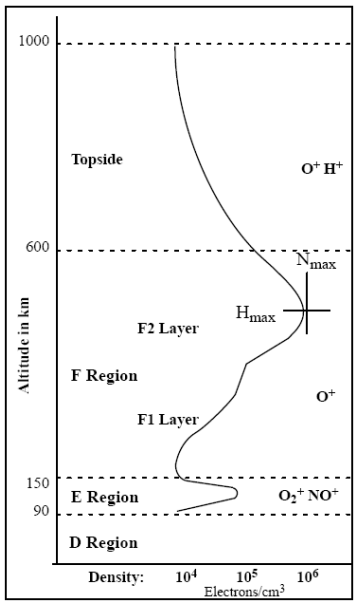

Figure 3.1 Describes the ionospheric layers and ions that are in each region (http://www.swpc.noaa.gov/info/Iono.pdf)

3.1.2. Sunspot Number

The condition of the ionosphere is directly related to the particles emitted from the Sun; therefore any changes occurring to the sun, such as sunspot variations, will results in changes to the ionosphere. Sunspots are areas with strong magnetic activity resulting in solar flares. These negatively charged electrons not only affect the ionization of the Earth's ionosphere but also disrupt radio transmissions and climate. At any given time, the number of sunspots is important to know as it directly correlates with the intensity of solar radiation. These dark patches on the Sun's surface have a reoccurring cycle of roughly 11 years. The last maximum occurred in the year 2000 (Seeber, 2003).

3.1.3. Ionospheric Effects on GPS Signal

Microwave signals passing through the ionosphere are influenced by free electrons from the ionization of gas molecules. As a result, the velocity of the carrier phase is increased by the same magnitude that the velocity of the pseudorange is delayed due to its dependency on the frequency. The ionosphere alters the ray path length typically causing errors ranging between several meters to about 20 m; however, at certain locations, and at a specified time and calendar year, this error can surpass 100 m (Hofmann-Wellenhof, 2008). The range error caused by this delay can easily be precisely determined with the utilization of a dual-frequency receiver (Liu et al., 2005). Another method of reducing the effect of the ionosphere is by the implementation of differential GPS; however, an increase in baseline length will also increase the residual for the ionospheric delay and may be of concern for high precision GPS applications. The phase and group ionospheric delay can be represented as:

$$D^{ION} = \pm \frac{40.3 * TEC}{f^2} \tag{3.1}$$

From the above equation, f is the carrier frequency and TEC is the total electron content along the signal path. D^{ION} is positive for the code pseudorange and negative for the phase pseudorange; both observables are a function of TEC. TEC is quantified in units of TECU, which represents 10^{16} electrons per metre squared:

$$TECU = 10^{16} \left(\frac{electrons}{m^2} \right) \tag{3.2}$$

TEC values are a function of many variables like the time of day, season, user location and magnetic activity. The highest daily value for TEC occurs at around 2:00 PM local time and the minimum value is obtained generally just before sunrise (Liao, 2000). Maximum TEC values take place at latitudes of about plus and minus 15°, north or south of the equator. By knowing the amount of TEC, a user can correct for the ionospheric delay.

To account for the delay induced by the ionosphere, various models have been developed including single-frequency Klobuchar model, dual-frequency combination, differential method and grid-based models. Due to the positional distortion cause by the ionosphere, selecting the right method is crucial when accurate GPS measurements are required. Discussed in further detail are the dual-frequency combination and the NOAA grid-based model.

3.1.4. Dual-frequency Combination

Due to the refractiveness of the ionosphere with respect to GPS signals, pseudorange measurements taken on L1 and L2 can be combined in order to approximate the ionospheric delay. The first order ionospheric slant delay determined on L1 is represented by:

$$D_{L1}^{ION} = \left(\frac{f_2^2}{f_1^2 - f_2^2}\right) \times (C2 - C1) \tag{3.3}$$

Where $C1$ and $C2$ are the code observables on L1 and L2. Using the above equation, the effect of the ionosphere can be largely removed from the original pseudorange observation. One drawback of using this linear combination is that the noise level is increased. When forming linear combinations, Teunissen and Keusberg (1998) found the measurement noise to be amplified by a factor of $2^{.5}$.

3.1.5. NOAA Ionospheric Grid

The National Oceanic and Atmospheric Administration (NOAA) is a federal agency which focuses on the conditions of oceans and the atmosphere. Information regarding the vertical and the slant United States total electron content (USTEC) can be downloaded from the NOAA website. TEC maps are produced in real-time using GPS observables from ground stations. A text file contains TEC values generated every 15 minutes. A compressed file containing TEC values over the course of a day can be accessed. The NOAA ionospheric grid ranges in latitude from 10˚ to 60˚ with TEC values for every one degree increment. The longitudinal direction varies from -150˚ to -50˚, also with one degree intervals. In addition to the TEC values, the compressed file contains the expected error in vertical TEC and the deviations of vertical TEC.

Generally, ionospheric grid maps are accurate to within 1 to 3 TEC units where 1 TEC unit is equivalent to approximately 0.1624 m (NOAA, 2009).

Since the TEC values for the latitude and longitude directions are given at intervals of one degree, linear interpolation was applied in order to obtain the TEC values for the geographic location of a specific station (see Figure 3.4). Next, a temporal interpolation method was implemented to match up the grid maps, sampled at every 15 minutes, with the collected data, sampled at every second. The spline interpolation function embedded in MATLAB was used to match the time resolutions. By extracting the station specific TEC value from the grid map and temporally interpolating the sampling interval to 1 second, an approximation for the ionospheric delay was obtained using Equation 3.1 and Equation 3.2.

$$y = y_o + (x - x_o)\left(\frac{y_1 - y_o}{x_1 - x_o}\right) \tag{3.4}$$

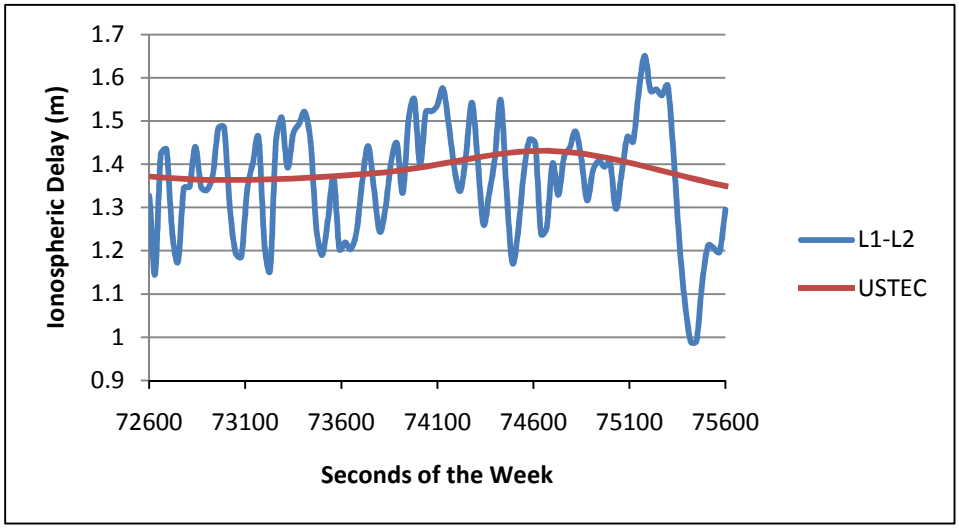

Figure 3.2 Ionospheric delay comparison between the dual-frequency combination (L1-L2) and the approximations from the NOAA ionospheric grid files (USTEC)

3.2. Multipath

Multipath is one of the most problematic errors affecting the accuracy of GPS positioning. This error is due to the signal reaching an antenna through two or more paths (see Figure 3.3). Most often, one of the signals received is obtained without any hindrance while the other signal or signals, which are generally weaker and often delayed, are reflected by surrounding features. The multipath effect is difficult to mathematically model due to its dependence on the environment where the antenna is located. The code and carrier measurements are both impacted by multipath to various degrees. The effect on P-code observations is two orders of magnitude larger than on carrier phase observations; while the C/A-code observations are at the order of several meters and can even surpass 100 m or more in extreme conditions (Seeber, 2003).

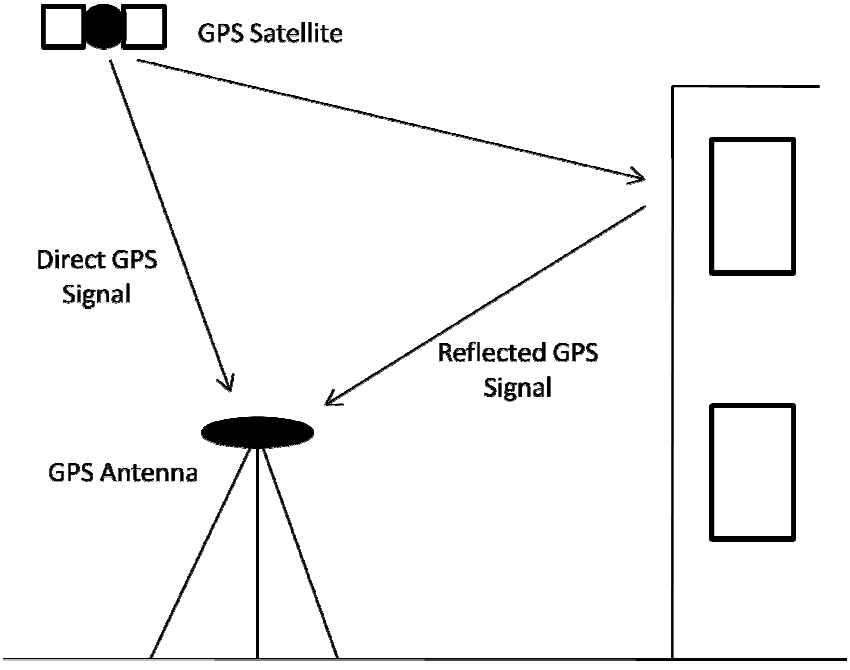

Figure 3.3 GPS signal affected by multipath

3.2.1. Reflection of GPS Signal

In general there are two main types of reflection, namely diffuse and specular. Diffuse multipath results from reflections caused by rough surfaces, while reflections from smooth surfaces are known as specular. In diffuse reflection when the signal comes into contact with the surface, it tends to scatter in all directions (see Figure 3.3). On the other hand, for the specular case, the surface condition causes a simple reflection where the angle of incidence is equal to the angle of reflection (see Figure 3.4); this results in a mirror-like reflection.

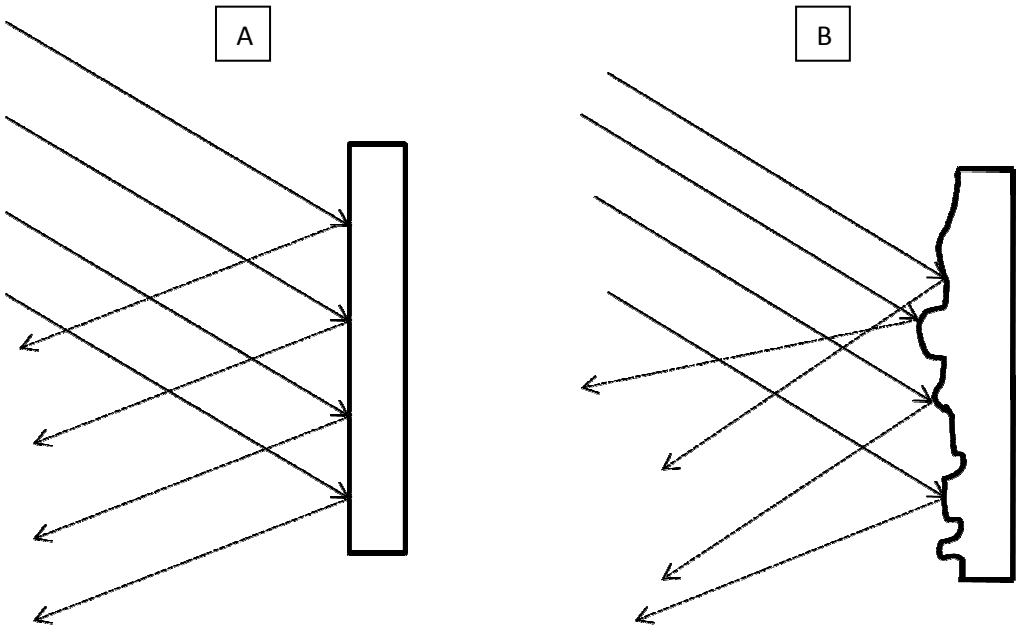

Figure 3.4 Specular reflection, A, and diffuse reflection, B

3.2.2. Signal Representation

The direct, reflected and received GPS signals can be modelled by (Hofmann-Wellenhof et al., 2008):

- **Direct signal:** $DS(\emptyset) = a \cdot cos\emptyset$ (3.5)
- **All Reflected signals:** $DF(\emptyset) = \sum \gamma \cdot a \cdot \cos(\emptyset + \Delta\emptyset)$ (3.6)
- **Received signal:** $R = DS(\emptyset) + DF(\emptyset)$ (3.7)

The parameters a represents the amplitude or power of the direct line-of-sight signal, $\emptyset$ and $\Delta\emptyset$ symbolize the phase and phase shifts, while γ is the damping factor. It can be seen here that the receiver processes the GPS signal through two paths: the direct signal and the indirect signals. Due to the fact the signal is being reflected, it will have phase offsets and a damping factor due to the reflection at the surface. The damping factor ranges from 0 to 1 where if $(\gamma = 0)$ then there is no reflection and $(\gamma = 1)$ implies that the reflected signals and the direct signal are equal in strength (Hofmann-Wellenhof et al., 2008).

3.2.3. Elevation Cut-Off

When trying to minimize multipath, site selection is absolutely critical as an area with lots of objects will be highly contaminated with multipath, while often an open area like a soccer field will have very little multipath; however, the latter scenario is not always possible. Eliminating satellites with low elevation angles is advisable as those particular satellites are more susceptible to multipath. Normally, a 15-degree cut-off elevation angle is implemented.

3.2.4. Signal-to-noise Ratio

The signal-to-noise ratio (SNR) for the GPS receiver can also be used as a measure to detect the presence of multipath. SNR is a function that relates the signal power (P) to the noise power (N):

$$SNR = 10 \log_{10} \frac{P}{N} \tag{3.8}$$

Cleaner signals have higher SNR values, therefore setting an appropriate tolerance level and rejecting signals with low SNR can be used to mitigate multipath. This receiver capability is referred to as the receiver's multipath rejection capability.

3.2.5. Hardware and Software Solutions

There are several hardware and software solutions available. At the hardware level, devices such as choke ring antennas and antennas with polarization discrimination technology are used to reject multipath. Choke ring antennas have become one of the most useful tools at mitigating multipath. This type of antenna blocks off multipath signals that reflect off surfaces below the antenna; but, signals reflected above the antenna from objects like buildings, are not removed. Choke ring antennas are very popular as many research studies have confirmed their effectiveness at suppressing multipath (Park et al., 2004).

In terms of software solutions, several techniques are available: the Narrow Correlator technique, the Multipath Elimination Technique (MET) and the Multipath Estimation Delay Lock Loop. In addition, several researchers have used a wavelet analysis approach to try to minimize the effects of multipath (see Section 1.1). Even though various multipath mitigation

techniques exist, examining methods to more effectively resolve the multipath error are still under investigation.

The TEQC software is able to calculate the multipath and the L1 frequency. Linearly combining Equations 2.1 and Equations 2.2 are possible. After some manipulation the multipath on L1 can be derived (MP1) and is given by:

$$MP1 = P_1 - \left(1 + \frac{2}{\omega - 1}\right)\Phi_1 + \left(\frac{2}{\omega - 1}\right)\Phi_2 \tag{3.9}$$

Where,

P is the measured code pseudorange (m)

Φ is the measured phase pseudorange (m)

ω is the ratio of the squared frequencies on L1 and L2 $\left(\frac{f_1^2}{f_2^2}\right)$

It is clear from Equation 3.9, that the value for MP1 can only be calculated using the code and carrier observables on L1 and L2.

4. Wavelet Theory

Fourier Analysis has been very popular at dealing with stationary signals where a signal is broken into sine and cosine waves of various frequencies. However, it is less useful in analysing non-stationary signals because Fourier Analysis is not localized in the time domain. To overcome this deficiency, another approach is required.

In the 1980s, Morlet and his team developed a method called wavelet transform to evaluate seismic data (Mertins, 1999). Since then, several different wavelets have emerged and the applications have widened. Wavelet breaks down signals to produce localized waves of varying durations, known as wavelets. Unlike sinusoids which extend from minus to plus infinity, wavelets have a limited duration (Fugal, 2007). Therefore, an event's frequency and location in time can be indicated by stretching and shifting the wavelet with respect to time so that it lines up with the desired event. Due to wavelets being localized in both the frequency and time domain via dilation and translation, it is, therefore, a good tool for analyzing non-stationary signals. Wavelet analysis decomposes a signal by passing two filters: high-pass and low-pass. The high-pass filter results in the extraction of detailed information, *d*, while approximation coefficients, *c*, are generated by the low-pass filter, (see Figure 4.1). Wavelets are used for audio denoising, signal compression, object detection, fingerprint compression, image denoising, image enhancement and more. In general, two types of wavelet transforms exist being continuous wavelet transform (CWT) and discrete wavelet transform (DWT).

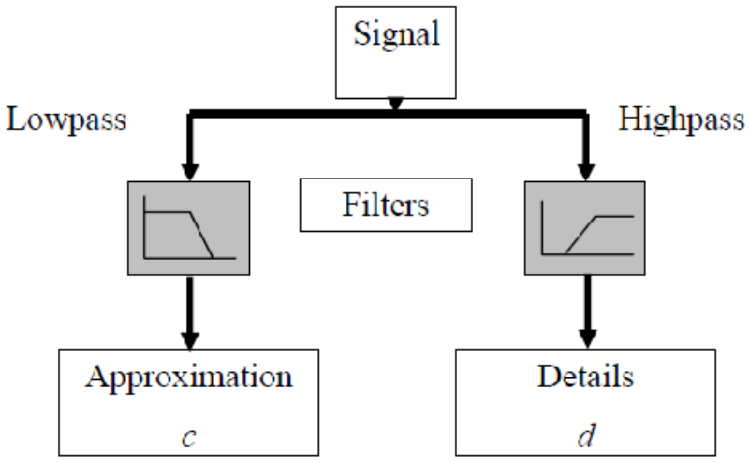

Figure 4.1 Low- and high-pass wavelet filters (from Elhabiby, 2007)

4.1. Continuous Wavelet Transform

The wavelet transform of a continuous signal is defined as (Daubechies, 1992):

$$(T^{wav}f)(a,b) = |a|^{-\frac{1}{2}} \int f(t)\psi\left(\frac{t-b}{a}\right)dt \tag{4.1}$$

$$\int \psi(t)dt = 0 \tag{4.2}$$

The parameter a represents the scale and b corresponds to the shift parameter. The term $|a|^{-\frac{1}{2}}$ is to ensure that the energy in the signal is preserved at every scale. Equation 4.2 must be satisfied. This means that by taking the inner product of $f(t)$ and the translated and scaled version of $\psi(t)$ leads to the computation of the wavelet transform.

The implementation of CWT often leads to excessive amount of redundant information as wavelet coefficients are calculated for every possible scale. To minimize computational processes, DWT is utilized (Mertins, 1999).

4.2. Discrete Wavelet Transform

The wavelet transform of a discrete signal, $f(t)$, is expressed as (Daubechies, 1992):

$$T_{m,n}^{wav}(f) = |a|^{-\frac{m}{2}} \int f(t)\psi(a_o^{-m}t - nb_o)dt \tag{4.3}$$

In the above equation, the integer valued variables m and n scale and dilate the mother function ψ to obtain wavelets. The wavelet's width is represented by the scale index m and its position is given by the location index n. Most often, the above equation uses a dyadic value for a and b. In general, once information is known regarding the mother functions, we can then extract everything about the approximations and details. The high-scale, low frequency part of the signal is the approximation, while the detail is the low-scale, high-frequency components (Aram et al., 2007).

One of the most important discoveries in the field of wavelet was made by Ingrid Daubechies who created a group of orthogonal wavelets. The Daubechies (db) family of wavelets is currently one of the most popular methods used and was impetus behind the practicality of discrete wavelet analysis (The MathWorks, 2009).

4.3. Multi-resolution Analysis

Multi-resolution analysis is a process where the signal can be expressed as a sum of constant multiples of a different set of fundamental signals. The signal is decomposed by passing it through a high-pass and low-pass filters, known as details and approximations. The high-pass filters analyze high frequencies in narrow windows, while the low-pass filters deal with low

frequencies in wider windows (see Figure 4.2). As a result, this is an effective method for removing non-stationary noise.

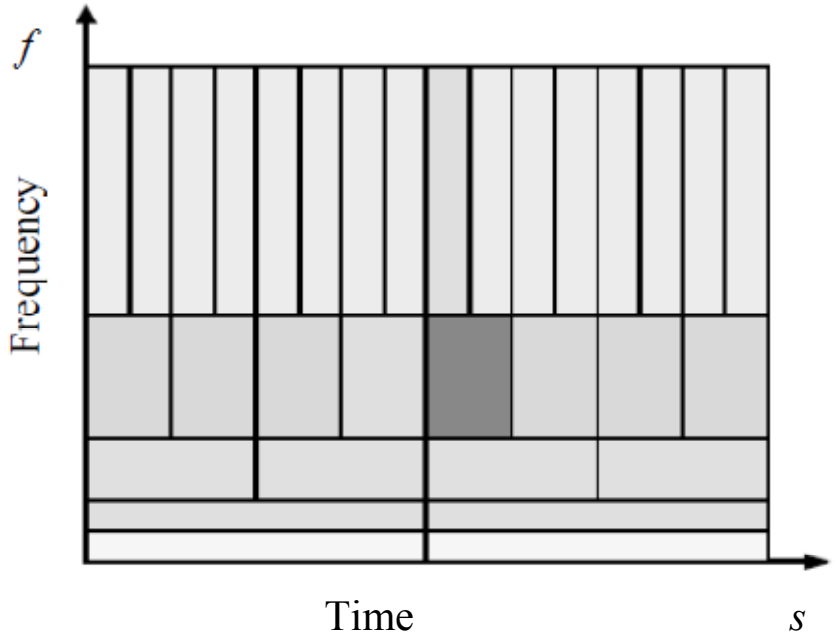

Figure 4.2 Multi-resolution Analysis (from Griffiths et al., 1997)

4.4. Multipath Correction using Wavelet Analysis

The multipath error for each respective satellite was approximated using wavelet analysis for each respective data set. The wavelet tool in MATLAB allowed us to isolate the multipath error. The approximated multipath values for each epoch were subtracted from the corresponding code pseudorange located in the original RINEX file for that session. For the static data, the db6 (level 7) wavelet was selected, while the db8 (level 9) wavelet was used for kinematic data. A new RINEX file was created with the multipath error essentially removed from the code observation. The above process was all coded in MATLAB.

4.5. Elimination of Multipath-Contaminated Satellites using Wavelet Analysis

Wavelet analysis was used to approximate the degree of multipath for each observed satellite. The respective standard deviations of the multipath estimates were then calculated. The satellites which demonstrated the largest spread were eliminated, and the best satellites were selected (see Section 6.1). The db8 (level 9) and db6 (level 7) wavelets were exclusively used for the kinematic and static data.

5. Data Collection

Static and kinematic data sets were collected on several different occasions to examine the performance of the low-cost GPS system. The data were acquired using single-frequency and dual-frequency receivers sampled at 1 Hz. Both receivers were connected to the same antenna using an antenna-splitter; the dual-frequency receiver collected the reference data. Static and kinematic modes were evaluated. For the static case, locations that possessed obstructions, like structures and sheets of metal, were selected in order to obtain multipath contaminated observables. For the kinematic sessions, areas with metallic objects were chosen and data was collected by moving around the object using a cart. In order to assess the quality of the multipath mitigation technique and to assert its consistency, several sets of data were collected in different environments. In all, three static locations and four kinematic sessions will be described in this chapter, as well as the equipment and software utilized.

Figure 5.1 Data collection equipment

5.1. Equipment

Two types of GPS receivers were used to collect data: a Trimble R7 dual-frequency receiver and an Ashtech AC12 single-frequency GPS receiver. Both receivers were connected to the same GPS antenna via an antenna splitter. The AC12 receiver was connected to a laptop where the data was stored using the Ashtech Geodetic Base Station (GBSS) software. On the other hand, for the dual-frequency receiver, the data were stored in its internal memory. Once the respective data collection sessions were over, the data obtained from each receiver were converted into the Receiver Independent Exchange (RINEX) format using the TEQC software. Once the data were converted into the RINEX format, analysis and manipulation of the data could then commence.

- **Trimble R7**

  The Trimble R7 GNSS dual-frequency system is a high accuracy GPS receiver. This receiver is capable of capturing modernized GPS and GLONASS signals. The unit also comes equipped with Bluetooth and UHF radio. This receiver is ideal for applications requiring high accuracy positioning, such as land surveying, construction, and others.

Figure 5.2 Trimble R7 Dual-frequency Receiver (from Trimble, 2009)

- **Ashtech AC12**

  The Ashtech AC12 is a single-frequency receiver capable only of obtaining code and carrier measurements. The AC12 receiver has the ability to track precise carrier phase while consuming low levels of power; this results in a cost-effective and reliable GPS receiver.

Figure 5.3 Ashtech AC12 Single-frequency Receiver (from ATEC, 2009)

5.2. Software

- **TEQC**

  TEQC is a software developed and maintained by the University of Navstar Consortium (UNAVCO) facility in Boulder, Colorado. Its name is derived from the software's three main functions: translation, editing and checking the quality of GPS and GLONASS data. This software was used to convert the data from the single- and dual-frequency receivers into the standard RINEX format. Edits to the data and quality checks were also performed. TEQC also has the capabilities of calculating multipath effects for dual-

frequency data. These values were used to validate multipath values obtained from wavelet analysis (Estey and Meertens, 1999).

- **MATLAB**

  MATLAB, which stands for MATrix LABoratry, is developed by The MathWorks, Inc. It is a technical computing language that allows the computation and visualization of problems and solutions. In this research, the Wavelet toolbox in MATLAB was extensively used for wavelet analysis. In addition, this software was used to analyze and manipulate RINEX data (MATLAB, 2009).

- **Trimble Total Control**

  Trimble Total Control (TTC) is a post-processing software developed by the Trimble Company, for GPS and GLONASS data. The software was used to process GPS data. Position estimates in static and kinematic environments were calculated using TTC. This software package can be used for: GPS baseline processing, geodetic network adjustments in one, two and three dimensions, and manual and automatic quality analysis (Trimble, 2009).

- **Bernese GPS Software**

  Bernese GPS software is widely used by research institutions worldwide, including Code Analysis Center (CODE) and Natural Resources Canada (NRCan). This software was developed and is maintained by the Astronomical Institute of the University of Bern since 1986. It is mainly used for precise geodetic and geodynamic applications and is capable

of processing GPS and GLONASS data. The software is normally used for static surveying, but can also be used for kinematic surveying.

5.3. Static Data Collection

- **Point MAY6**

  The first GPS data set was collected on May 6, 2009. Both the AC12 single-frequency and R7 dual-frequency receivers connected via an antenna splitter, logged data for approximately 1 hour. The GPS antenna was set-up in a backyard approximately 2 m away from a brick wall (see Figure 5.4). Other obstructions like fences and trees were also present nearby.

Figure 5.4 MAY6 station set-up

- **Point JU3A**

  Another static data set was collected in the morning of June 3, 2009 to evaluate the performance of receivers in a different environment. This time the GPS antenna was set-up near a metallic structure with groves about 2 m away. No other significantly large objects were nearby (see Figure 5.5).

Figure 5.5 JU3A station set-up

- **Point JU3B**

  During the last data collection session, which took place during the afternoon of June 3, 2009, the GPS equipment was placed near a flat metallic sheet, again nearly 2 m away. The purpose of collecting data at this point was to evaluate a different type of metallic structure (see Figure 5.6).

Figure 5.6 JU3B station set-up

5.4. Kinematic Data Collection

- **Session KSEP9**

  A kinematic data set was collected in the early morning on September 9, 2009 in a parking lot. This site was selected based on the presence of a metallic trailer (see Figure 5.7). The GPS equipment was placed securely in a shopping cart. Static data was first collected for approximately 60 minutes. After that, the cart was put into motion and low dynamic kinematic data was then gathered. The closest the cart was brought to metallic structure was about 5 m. The trajectory is depicted by Figure 5.8.

Figure 5.7 KSEP9 session set-up

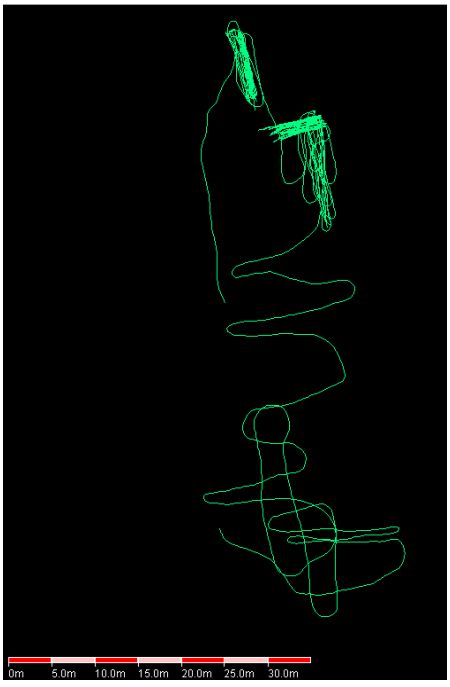

Figure 5.8 KSEP9 session trajectory

- **Session KJU27**

  On July 27, 2009, GPS data was collected in a parking lot at Humber College. GPS equipment consisting of three receivers and two antennas were set-up and softly put into a cart (see Figure 5.9). One Trimble R7 and one AC12 receivers were connected to a common antenna via an antenna splitter. Another AC12 receiver was connected directly to a second antenna to evaluate the performance of the AC12 single-frequency antenna. The data from the AC12 receivers were collected on separate laptops powered by external battery sources while the R7 receiver stored data internally. Approximately 90 minutes of data collected. During the session, the cart was brought to a maximum of roughly 5 m of the metallic object.

Figure 5.9 Kinematic data collection cart with the metallic structure for the KJU27 session

A base station was set-up approximately 200 m from the metallic structure (see Figure 5.10). The antenna was mounted on top of a concrete pillar. This monument control point was set-up by the Geodetic Survey Division and is a part of the Canadian Base Network. Figure 5.11 shows the data collection path.

Figure 5.10 Base station set-up for the KJU27 session

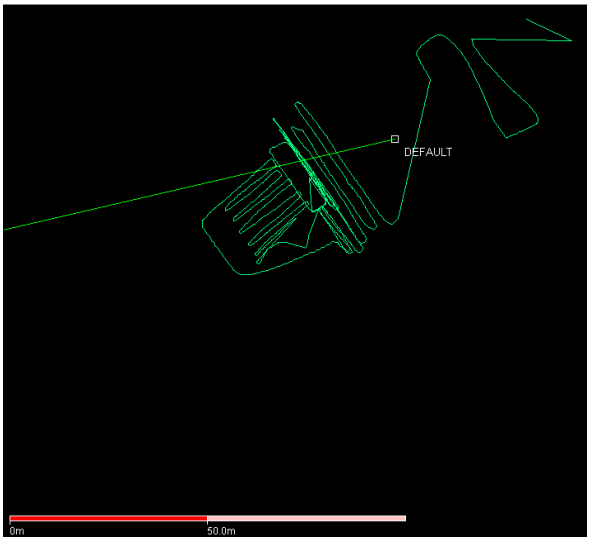

Figure 5.11 KJU27 session trajectory

- **Session KM8A**

  Just past midnight on May 8, 2009, a kinematic data set was collected for both the single and dual-frequency receivers in a housing subdivision. Approximately 90 minutes of data was collected. The GPS antenna was placed on the roof of a vehicle using a magnetic mount. Along the data collection path, there were many towering trees, houses and vehicles. Figure 5.12 shows the trajectory taken during the session.

Figure 5.12 KM8A session trajectory

- **Session KM8B**

  Kinematic data set for the KM8B session was collected on May 8, 2009 for approximately 45 minutes. The R7 and AC12 receivers were connected to the same antenna via an antenna splitter. Many features were present along the vehicles trajectory including trees, vehicles and buildings (see Figure 5.13).

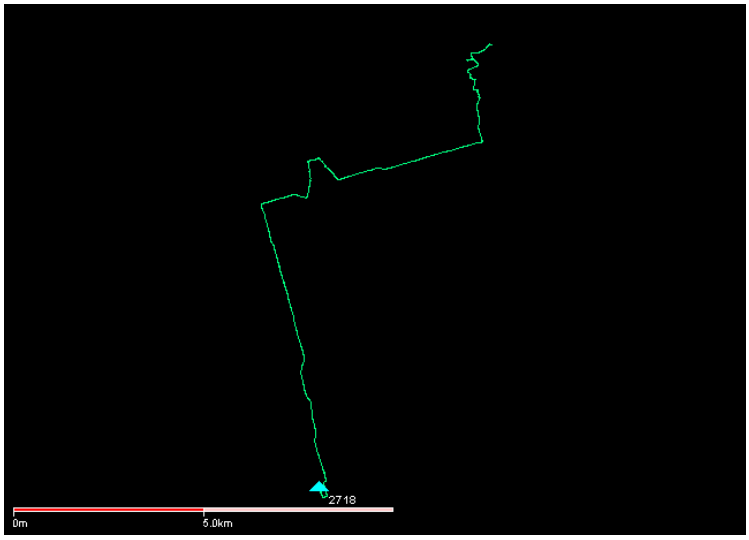

Figure 5.13 KM8B session trajectory

6. Analysis

Once the data were collected, it were converted into RINEX format and then analysed. Described in this section, are the steps taken through the analysis process.

6.1. Wavelet Selection

Once the code observable was subtracted from the phase observable and the ionospheric delay and the ambiguity term were accounted for, all that essentially remained was the low-frequency multipath and high-frequency noise (see Section 2.2.3). Wavelet analysis was then employed in order to separate the low- and high- frequencies. Wavelet is a tool which provides localization in both the time and frequency domain. Before applying wavelet analysis, it is first necessary to select a family of wavelets.

One of the most widely used wavelets is the Daubechies family of wavelets. The Daubechies wavelet transform is named after the Belgian physicist and mathematician, Ingrid Daubechies. She developed a family of orthogonal wavelets which are extensively used in wavelet analysis. Due to its superior ability when compared to other wavelets in signal processing, the family of Daubechies wavelets was selected as the mother wavelet for this research.

In order to select an appropriate mother wavelet (db) and its level, wavelet approximations for the Daubechies family were generated from db4 to db9 and (levels) 5 to 9. These wavelets were evaluated based on the accuracy of their position estimate. Once the low-

frequency multipath estimates were extracted using the Daubechies wavelets, the multipath approximation values were used to correct the code observable. Next, position estimates for each respective wavelet were compared with the reference position obtained using data from the R7 Trimble dual-frequency receiver.

For the static stations, the difference between the position based on the Daubechies wavelet estimates and the reference position, the root mean square error (RMSE), were calculated. The best wavelet was selected based on the Daubechies wavelet and level which consistently demonstrated the smallest RMSE for all three static stations (see Figure 6.1). For the kinematic sessions, differences between the results and reference values were obtained. The mother wavelet and level combination that consistently displayed the lowest standard deviation in the KM8A and KM8B sessions was selected (see Figure 6.2).

Separate wavelets were selected for the static and kinematic modes due to the different dynamics, since the former is at rest and the latter is in motion. The complete tables are located in Appendix A. Overall, the db6 (level 7) wavelet for the static trials and db8 (level 9) for the kinematic sessions were the most effective.

Table 6.1 RMSE for the top ten Daubechies mother wavelets (db) and levels (L) for the MAY6, JU3A and JU3B static trials

May-06	
Wavelet	**RMSE (m)**
db6 L7	0.023
db7 L6	0.024
db9 L7	0.024
db5 L7	0.024
db4 L6	0.025
db8 L6	0.025
db4 L5	0.026
db7 L5	0.026
db8 L5	0.026
db5 L5	0.026

JU3A	
Wavelet	**RMSE (m)**
db4 L8	0.008
db7 L7	0.010
db7 L8	0.011
db5 L8	0.013
db4 L7	0.014
db6 L7	0.015
db8 L8	0.015
db9 L8	0.017
db8 L7	0.018
db6 L8	0.020

JU3B	
Wavelet	**RMSE (m)**
db6 L8	0.016
db5 L8	0.018
db7 L7	0.018
db9 L8	0.019
db4 L7	0.019
db6 L7	0.020
db7 L8	0.021
db8 L5	0.021
db4 L8	0.021
db7 L6	0.021

Table 6.2 Standard deviations for the top ten Daubechies mother wavelets (db) and levels (L) for the KM8A session

dX	
Wavelet	**STD (m)**
db4 L9	0.108
db8 L9	0.122
db5 L9	0.125
db9 L9	0.126
Db7 L9	0.130
db6 L9	0.149
db4 L8	0.149
db8 L8	0.153
db9 L8	0.153
db5 L8	0.156

dY	
Wavelet	**STD (m)**
db4 L9	0.106
db8 L9	0.125
db9 L9	0.126
db5 L9	0.126
db7 L9	0.135
db6 L9	0.150
db9 L8	0.152
db5 L8	0.154
db4 L8	0.154
db8 L8	0.158

dZ	
Wavelet	**STD (m)**
db4 L9	0.437
db9 L9	0.452
db5 L9	0.457
db8 L9	0.458
db7 L9	0.472
db6 L8	0.473
db6 L9	0.479
db9 L8	0.488
db5 L8	0.490
db7 L8	0.490

Table 6.3 Standard deviations for the top ten Daubechies mother wavelets (db) and levels (L)

KM8B session

dX	
Wavelet	**STD (m)**
db7 L9	0.186
db6 L9	0.315
db8 L9	0.625
db4 L9	0.813
db9 L9	1.044
db5 L9	1.062
db9 L8	1.369
db4 L8	1.400
db5 L8	1.409
db8 L8	1.447

dY	
Wavelet	**STD (m)**
db7 L9	0.191
db6 L9	0.350
db8 L9	0.722
db4 L9	0.940
db9 L9	1.219
db5 L9	1.236
db9 L8	1.604
db4 L8	1.639
db5 L8	1.651
db8 L8	1.697

dZ	
Wavelet	**STD (m)**
db6 L9	0.605
db7 L9	0.680
db5 L9	0.701
db9 L9	0.722
db8 L9	0.744
db4 L9	0.783
db9 L8	0.790
db8 L8	0.801
db5 L8	0.810
db4 L8	0.813

6.2. Application of Wavelet

Wavelets db6 (level 7), for the static stations, and db8 (level 9), for the kinematic sessions, were chosen to separate the high and low frequencies from Equation 2.6. The Discrete Wavelet Transform (DWT) application in MATLAB's Wavelet Toolbox was employed to generate approximations for the low-frequency multipath.

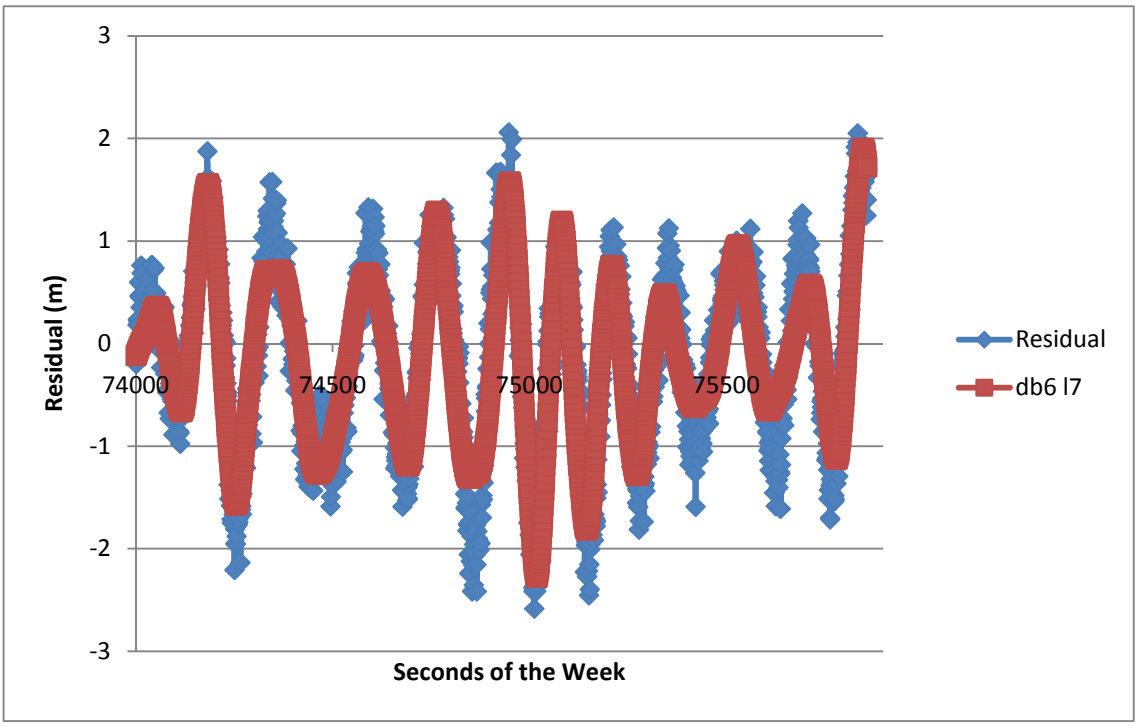

Figure 6.1 Comparison between the residual consisting of essentially multipath and noise with the wavelet approximation for the Daubechies wavelet db6 (level 7)

The isolated multipath estimates from wavelet analysis was compared with the reference multipath value generated using TEQC. Figure 6.2 demonstrates that a strong relationship exists between multipath values approximated by wavelet, and the reference multipath value outputted by the TEQC software.

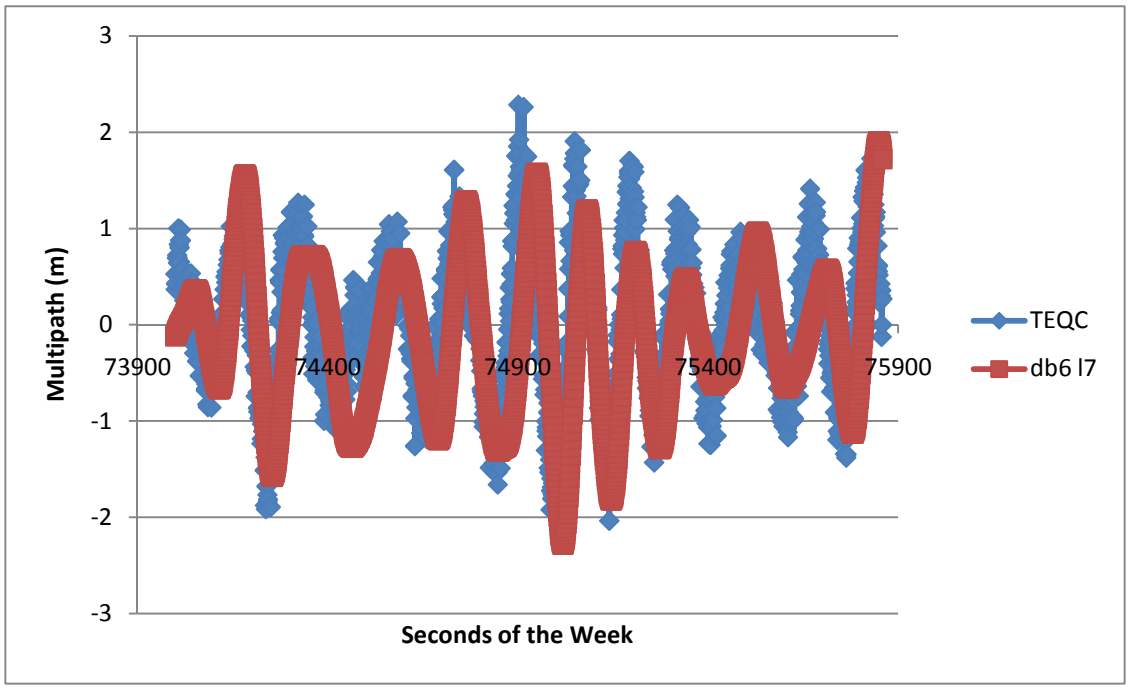

Figure 6.2 Comparison between multipath values obtained from TEQC and approximated by the Daubechies wavelet db6 (level 7)

6.3. Multipath Correction using Wavelet Analysis

Wavelet approximations were used to adjust observations for all the satellites. Once the low-frequency multipath estimates were extracted for each satellite using the Daubechies wavelets, these values were then subtracted from each coinciding code observations for each specific satellite in the respective RINEX files. A MATLAB code was created to manipulate and modify the original RINEX file resulting in a new RINEX file containing essentially multipath corrected observations. Position estimates were then obtained with these files using TTC and Bernese GPS software for both static and kinematic data.

6.4. Elimination of Satellites

For the static data, wavelet analysis was used as a tool to identify satellites that were severely contaminated with multipath. The satellites were then removed and a new RINEX file was created containing the best satellites. First, the Daubechies wavelet estimates of multipath were obtained for each satellite. The standard deviations were then calculated for each approximation. The satellites with the largest standard deviations were removed. A new RINEX file was generated and processed to obtain a position estimate.

Tables 6.4 and 6.5 describe the standard deviation, elevation and azimuth associated with each satellite for the respective static and kinematic session. In general, the satellites with the highest elevation resulted in the least amount of multipath represented by the small standard deviations. Satellites closer to the horizon, and with a line-of-sight that interacts with the environment, were identified to have the highest degree of multipath indicated by the large standard deviations. For the MAY6 station, the GPS antenna was set-up north of the multipath inducing rectangular object (see Figure 6.3).

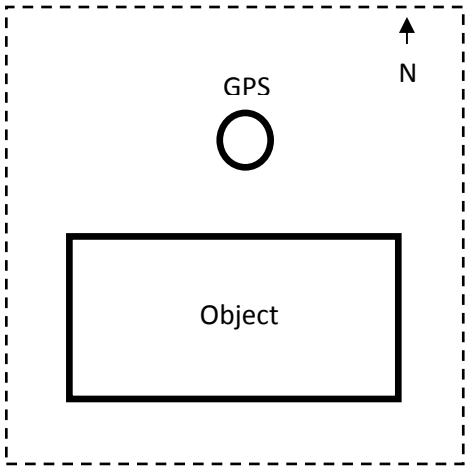

Figure 6.3 GPS set-up for the MAY6 station

Since the object was rectangular in shape, satellites with a low elevation and an azimuth of 0˚ to 90˚ and 270˚ to 360˚ were expected to experience significant multipath; this is what resulted, Table 6.4.

Table 6.4 Demonstrates the satellites elevation, azimuth and the standard deviation (STD) of multipath generated for each satellite (SVN) in view for the MAY6 station

MAY6			
SVN	**STD (m)**	**Elevation**	**Azimuth**
26	0.428	59˚	185˚
15	0.498	75˚	116˚
29	0.608	38˚	217˚
24	0.657	78˚	124˚
18	0.722	29˚	268˚
10	0.982	30˚	70˚
6	1.655	4˚	328˚
21	1.940	54˚	304˚
27	5.079	20˚	136˚
8	5.282	14˚	43˚

For the kinematic session KJU27, the instance where the GPS antenna was east of the metallic object was evaluated (see Figure 6.4). The satellites expected to have the highest degree of multipath would have an azimuth of about 0˚-180˚; the results in Table 6.5 supported the hypothesis.

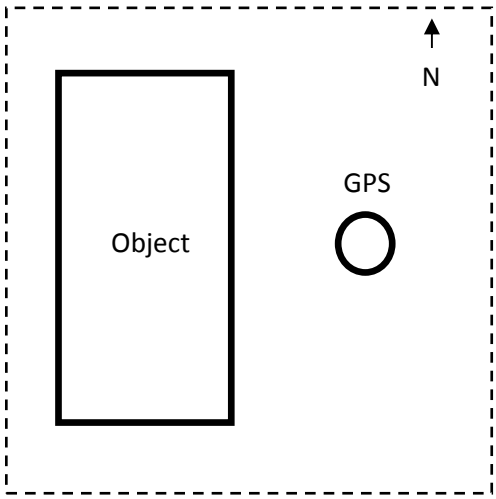

Figure 6.4 GPS set-up for the KJU27 session

Table 6.5 Demonstrates the satellites elevation, azimuth and the standard deviation (STD) of multipath generated for each satellite (SVN) in view for the KJU27 session

KJU27			
SVN	**STD (m)**	**Elevation**	**Azimuth**
3	0.938	45˚	266˚
14	1.384	51˚	268˚
26	1.406	69˚	30˚
22	1.460	75˚	316˚
6	2.433	34˚	156˚
9	2.794	48˚	158˚
12	3.936	15˚	114˚
21	7.101	18˚	177˚
27	16.556	32˚	48˚
19	29.316	7˚	90˚
31	33.249	5˚	207˚
30	41.046	7˚	144˚

7. Results

Presented in this chapter are the positioning results obtained after the application of wavelet analysis and the post-processing software. The static and kinematic data were processed using the TTC and Bernese scientific softwares. Data from the Ashtech AC12 single-frequency receiver was compared with the reference data obtained from the Trimble R7 dual-frequency receiver. Both receivers logged data simultaneously at the same rate. Comparisons in position are made between the processing of the original file, corrected data using multipath approximations file, and removal of multipath contaminated satellites file.

7.1. Static Results

Data for each static station was processed using both TTC and Bernese GPS software packages for the two different methods including the original file. The results for stations MAY7, JU3A and JU3B were graphed (see Figures 7.1 to 7.6) and tabulated (see Tables 7.1 to 7.6). Out of the two types of methods, the best position estimates were consistently obtained from processing the file with the multipath contaminated satellites removed.

In general improvements in the horizontal and vertical components of position were achieved when satellites were eliminated. A maximum of 86% improvement in the RMSE was obtained when this method and the RMSE from the original file were compared. Moreover, significant improvements in the Z direction were consistently demonstrated. The wavelet correction method did demonstrate slight positioning improvement for the MAY6 and JU3B stations, while significant improvement was obtained for the JU3A station with a 78% RMSE

when comparing this method to the original file. Overall from the figures and tables in this section pertaining to position solutions obtained from the Bernese and TTC softwares, the superiority of Bernese GPS software was displayed by better position outputs when compared to TTC. The below graphs and tables in this section, relating to specific stations and sessions, are described.

- **Station MAY6**

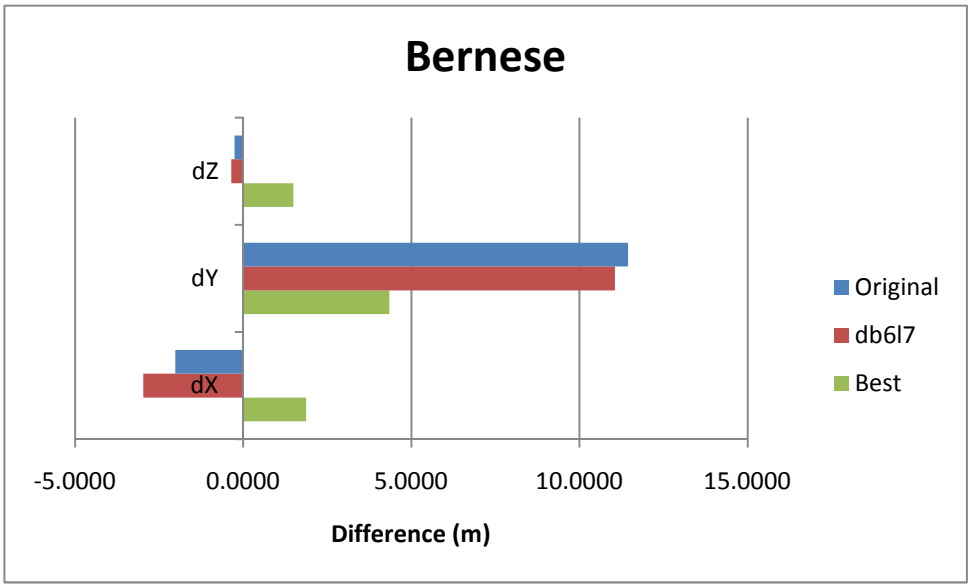

Figure 7.1 Differences in position estimates between the original (Original), multipath corrected (db6L7) and selection of best satellites (Best) files when compared with the reference data for the MAY6 station processed by Bernese

Table 7.1 Differences in the XYZ components and RMSE values between the original (Original), multipath corrected (db6L7) and the selection of best satellites (Best) files when compared with the reference data for the MAY6 station processed by Bernese

Bernese				
	dX (m)	**dY (m)**	**dZ (m)**	**RMSE (m)**
Original	-2.021	11.441	-0.260	11.621
db6L7	-2.966	11.052	-0.357	11.448
Best	1.874	4.344	1.495	4.962

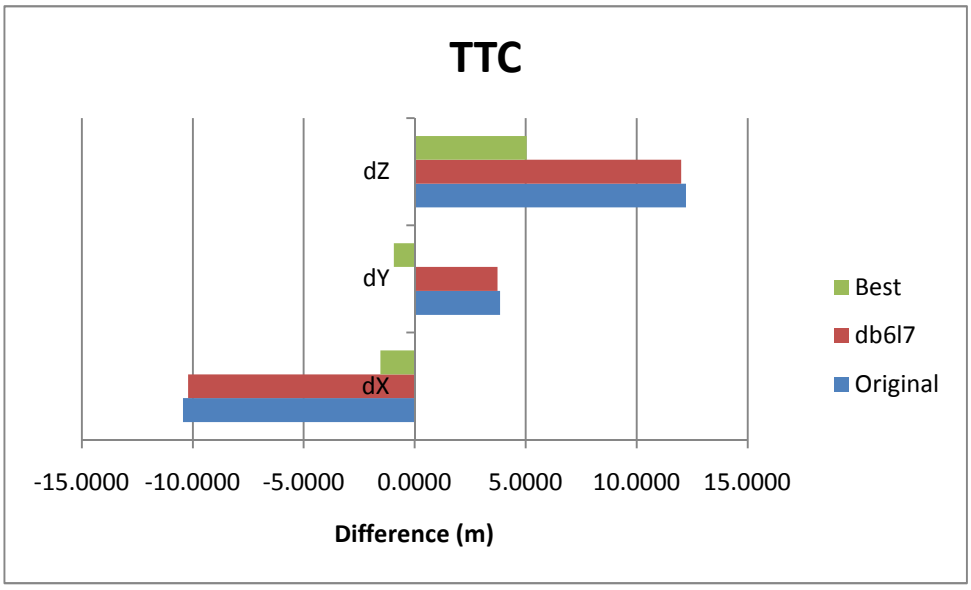

Figure 7.2 Differences in position estimates between the original (Original), multipath corrected (db6L7) and the selection of best satellites (Best) files when compared with the reference data for the MAY6 station processed by TTC

Table 7.2 Differences in the XYZ components and RMSE values between the original (Original), multipath corrected (db6L7) and the selection of best satellites (Best) files when compared with the reference data for the MAY6 station processed by TTC

TTC				
	dX (m)	**dY (m)**	**dZ (m)**	**RMSE (m)**
Original	-10.447	3.848	12.221	16.532
db6L7	-10.212	3.723	12.010	16.198
Best	-1.546	-0.940	5.047	5.362

Figures and Tables 7.1 and 7.2 demonstrate the results obtained when comparing the reference data with the original, multipath corrected and best satellites files. A slight improvement was achieved when code observations in the original RINEX file were modified using the approximated multipath values from wavelet analysis. The biggest improvements were obtained with best satellites methods where multipath contaminated satellites are identified and those satellites which displayed the biggest standard deviations were removed. Improvements in the RMSE of approximately 68% and 57 % were achieved when the removal of multipath contaminated satellites method was compared with the original RMSE for TTC and Bernese softwares, respectively. Slight advances of 2 % and 1.5% for TTC and Bernese were obtained when the corrected multipath RMSE was compared with the original RMSE for TTC and Bernese.

- **Station JU3A**

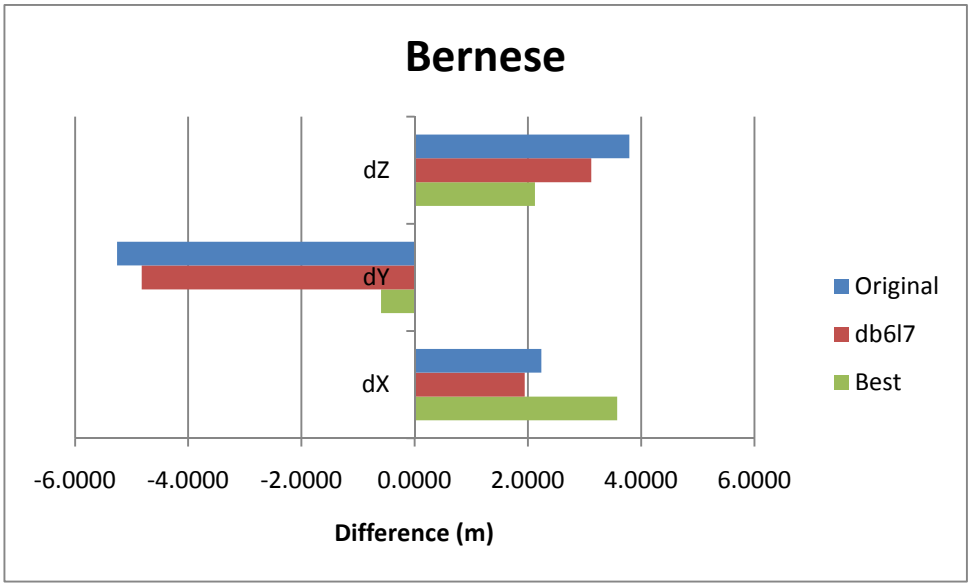

Figure 7.3 Differences in position estimates between the original (Original), multipath corrected (db6L7) and the selection of best satellites (Best) files when compared with the reference data for the JU3A station processed by Bernese

Table 7.3 Differences in the XYZ components and RMSE values between the original (Original), multipath corrected (db6L7) and the selection of best satellites (Best) files when compared with the reference data for the JU3A station processed by Bernese

Bernese				
	dX (m)	**dY (m)**	**dZ (m)**	**RMSE (m)**
Original	2.236	-5.256	3.788	6.854
db6L7	1.945	-4.821	3.120	6.063
Best	3.578	-0.594	2.122	4.202

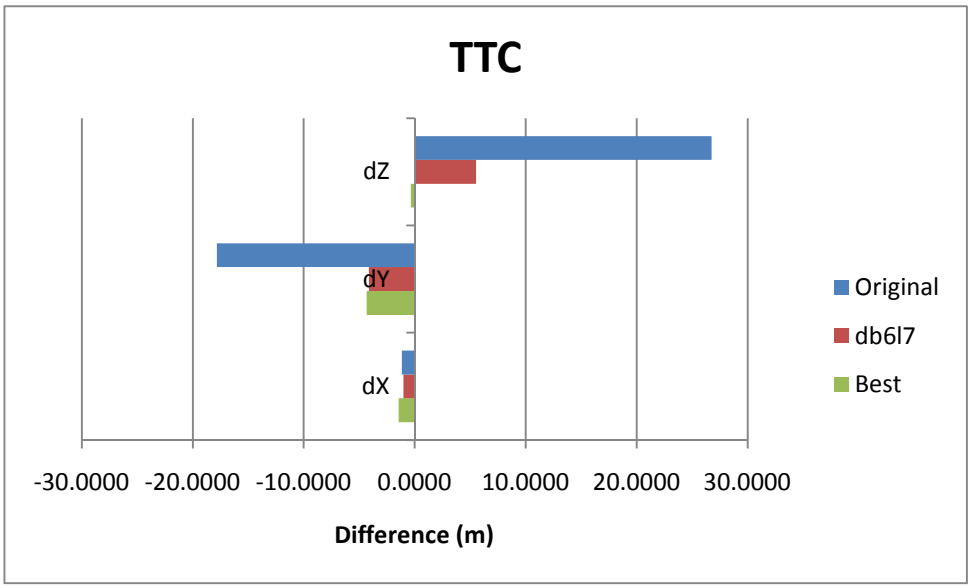

Figure 7.4 Differences in position estimates between the original (Original), multipath corrected (db6L7) and the selection of best satellites (Best) files when compared with the reference data for the JU3A station processed by TTC

Table 7.4 Differences in the XYZ components and RMSE values between the original (Original), multipath corrected (db6L7) and the selection of best satellites (Best) files when compared with the reference data for the JU3A station processed by TTC

TTC				
	dX (m)	**dY (m)**	**dZ (m)**	**RMSE (m)**
Original	-1.171	-17.831	26.734	32.156
db6L7	-1.029	-4.130	5.539	6.985
Best	-1.451	-4.323	-0.350	4.573

Figures 7.3 and 7.4 and Tables 7.3 and 7.4 demonstrate the results obtained when comparing the reference data with three different types of files: original (Original), multipath corrected (db6L7), and best satellites (Best). Significant improvements of 78% and 86% in the RMSE were observed when comparing the RMSE of the multipath corrected and best satellites with the original RMSE for the TTC software, Figure 7.4. A significant improvement in position was displayed using the Bernese software (see Figure 7.3). Improvements of 12% and 39% in the RMSE were observed when the RMSE of the multipath corrected and best satellites data was compared with the original RMSE for the Bernese software.

- **Station JU3B**

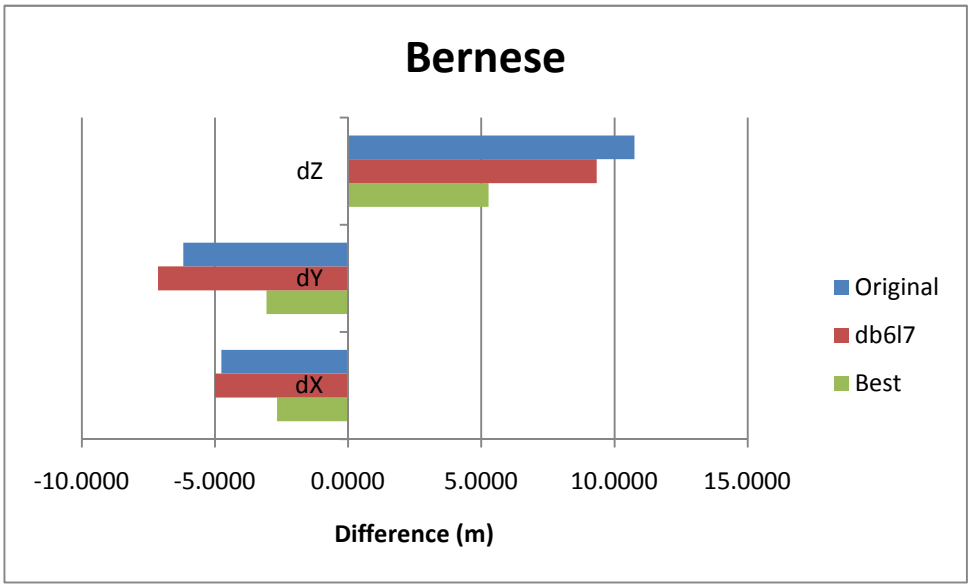

Figure 7.5 Differences in position estimates between the original (Original), multipath corrected (db6L7) and the selection of best satellites (Best) files when compared with the reference data for the JU3B station processed by Bernese

Table 7.5 Differences in the XYZ components and RMSE values between the original (Original), multipath corrected (db6L7) and the selection of best satellites (Best) files when compared with the reference data for the JU3B station for Bernese

Bernese				
	dX (m)	dY (m)	dZ (m)	RMSE (m)
Original	-4.755	-6.187	10.747	13.281
db6L7	-4.995	-7.137	9.327	12.763
Best	-2.665	-3.067	5.267	6.652

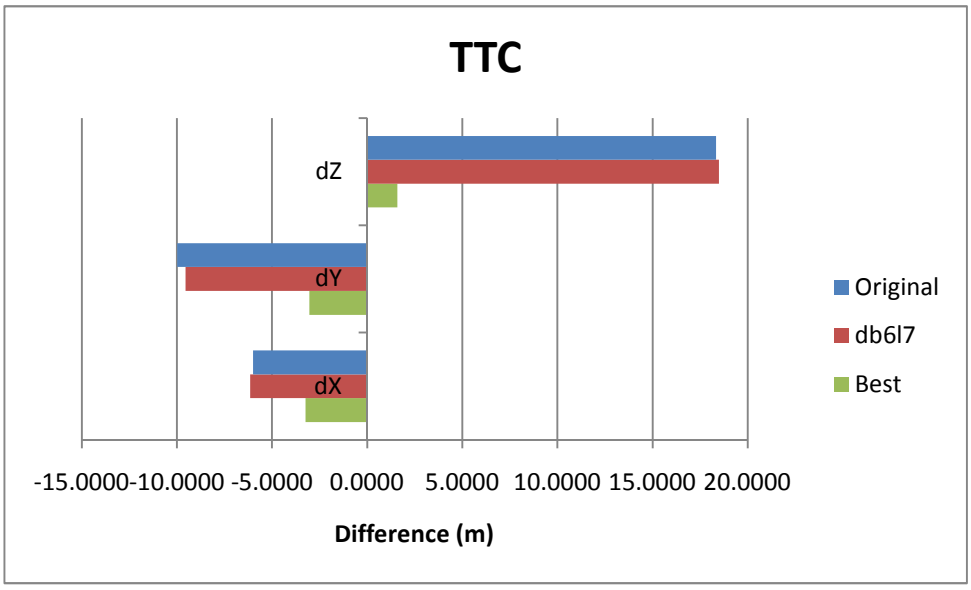

Figure 7.6 Differences in position estimates between the original (Original), multipath corrected (db6L7) and the selection of best satellites (Best) files when compared with the reference data for the JU3B station processed by TTC

Table 7.6 Differences in the XYZ components and RMSE values between the original (Original), multipath corrected (db6L7) and the selection of best satellites (Best) files when compared with the reference data for the JU3B station processed by TTC

TTC				
	dX (m)	dY (m)	dZ (m)	RMSE (m)
Original	-6.005	-9.983	18.335	21.723
db6L7	-6.147	-9.537	18.490	21.694
Best	-3.246	-3.044	1.580	4.722

Figures and Tables 7.5 and 7.6 demonstrate the results obtained when comparing the reference data with three methods: original (Original), multipath corrected (db6L7), and best satellites (Best). Similar to station MAY6, the multipath corrected demonstrated a slight improvement while the best satellites had the biggest impact for the TTC and Bernese, respectively (see Figures 7.5 and 7.6). Improvements of 4% and 48% in the RMSE were observed when comparing the original data to the multipath corrected and best satellites using Bernese; while for same files, TTC displayed improvements with respects to the RMSE of 1% and 78%, respectively.

7.2. Kinematic Results

Wavelet analysis was performed for the KJU27 and KSEP9 kinematic sessions. The Daubechies wavelet db8 (level 9) was exclusively used. A new RINEX file was created containing code observations with multipath essentially removed based on wavelet analysis.

Additionally, the satellites severely contaminated with multipath were removed based on the standard deviations of multipath approximations. Position estimates for each epoch were obtained.

- **KJU27 session**

The kinematic data collected during the KJU27 session were analyzed and then processed using TTC. A baseline of less than 2 km was formed using base station coordinates obtained from a site maintained by Leica Geosystems Limited. Comparisons were made between the position results from the multipath corrected, the selection of the best satellites and the original files. The results were observed and are discussed in this section. Details regarding the equipment and KJU27 session are given in Chapter 5.

Table 7.7 represent the results obtained from processing the original RINEX file with unmodified C1 observations. The differences in positions had standard deviations of below 3 cm for the horizontal positions, and approximately 6 cm for the vertical position. These numbers indicated that there is not a significant difference between the two data sets. In Figure 7.7, jumps are observed in all of the three components. This was caused by a loss of lock on satellites which is caused by a reduction in the field of view for the GPS antenna as result of the metallic object and the high degree of multipath experienced by the antenna (Hofmann-Wellenhof et al., 2008).

Table 7.7 Statistical information for the differences in XYZ position components between the original data and reference data for KJU27 session

	Mean (m)	STD (m)	Max (m)	Min (m)
dX	-0.205	0.026	-0.143	-0.408
dY	-0.195	0.030	-0.139	-0.353
dZ	-1.461	0.062	-1.088	-1.645

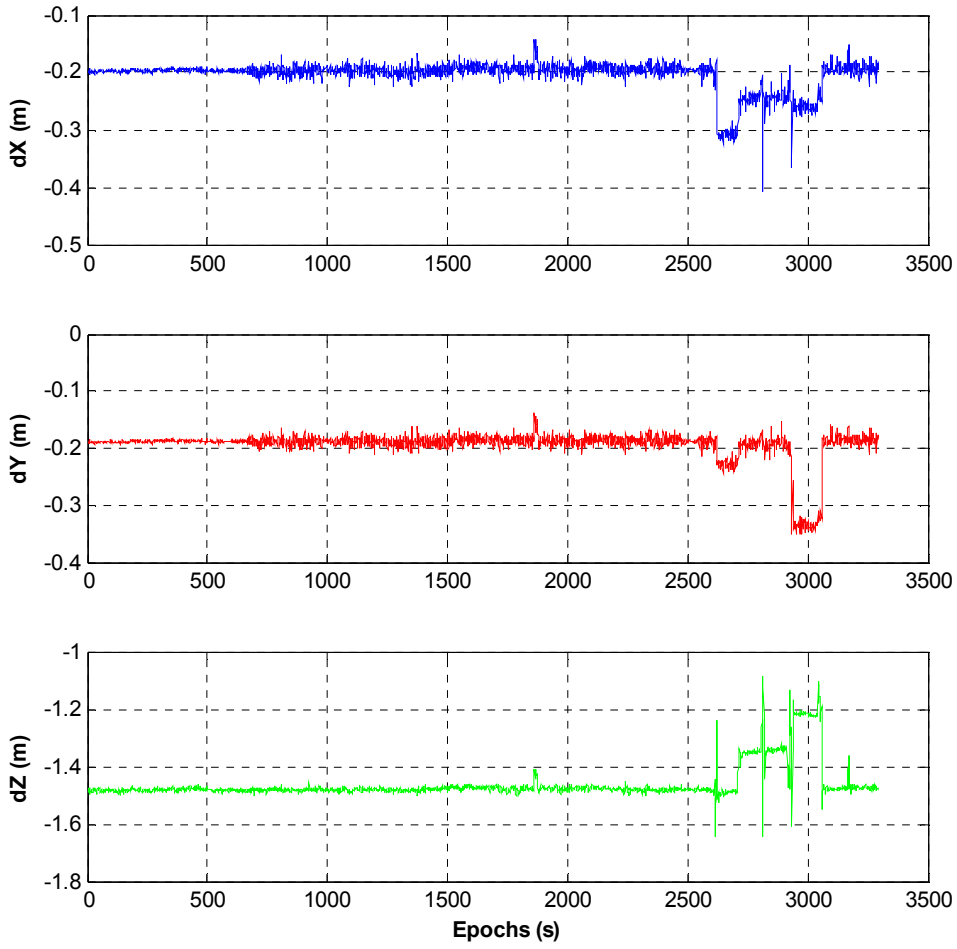

Figure 7.7 Differences in XYZ position components between the original data and reference data for the KJU27 session

Figure 7.8 depict the results generated by processing the multipath corrected file. The approximated multipath value from wavelet analysis was subtracted from the raw code observation. When compared to Figure 7.7, the jumps have increased surpassing 1 m. These jumps affect the code minus carrier linear combination. The loss of lock on satellites causes the instability in the residual of the ambiguities. The below table, Table 7.8, indicates standard deviations in the decimetre range.

Table 7.8 Statistical information for the differences in XYZ position components between the multipath corrected data and reference data for the KJU27 session

	Mean (m)	STD (m)	Max (m)	Min (m)
dX	-0.199	0.185	1.479	-0.580
dY	-0.172	0.236	0.836	-0.683
dZ	-1.076	0.871	2.169	-2.634

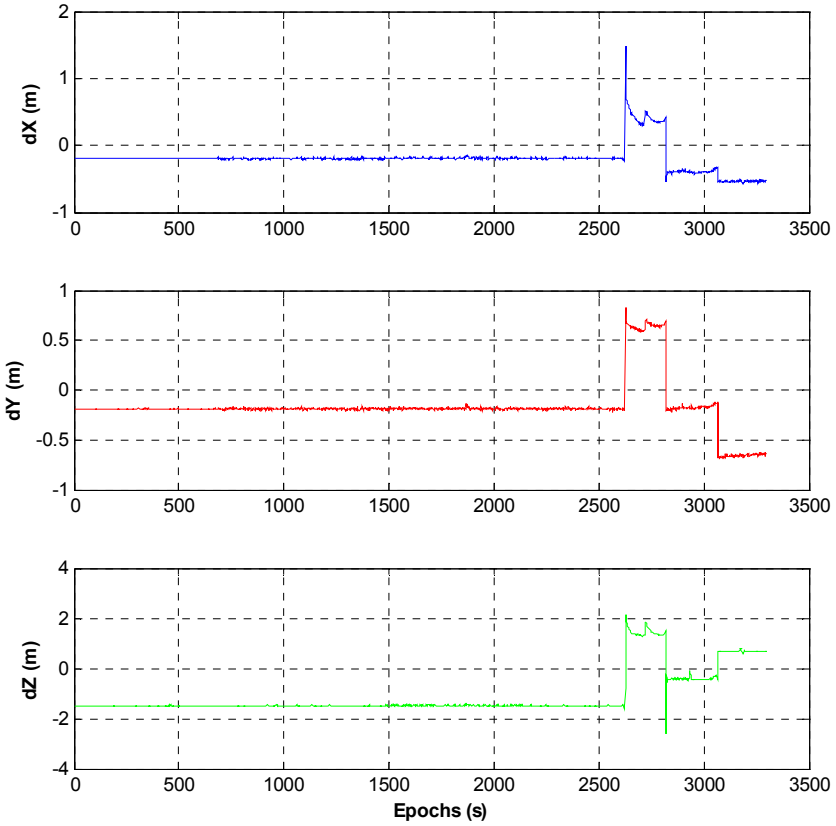

Figure 7.8 Differences in XYZ position components between the multipath corrected data and reference data for the KJU27 session

Table 7.9 show the results from processing of the best satellites by eliminating those satellites with the highest degree of multipath based on wavelet analysis. Decimetre-level standard deviations are obtained for the horizontal positions while the vertical component had deviations near 1 m. In Figure 7.9, the jumps have further increased when compared to Figures 7.7 and 7.8. The elimination of satellites is generally not recommended in kinematic mode as there is generally already a low redundancy due to satellites coming in out of sight.

Table 7.9 Statistical information for the differences in XYZ position components between the selection of best satellites and reference data for the KJU27 session

	Mean (m)	STD (m)	Max (m)	Min (m)
dX	0.108	0.418	1.923	-0.227
dY	0.080	0.324	1.266	-0.212
dZ	-0.732	1.081	6.607	-1.512

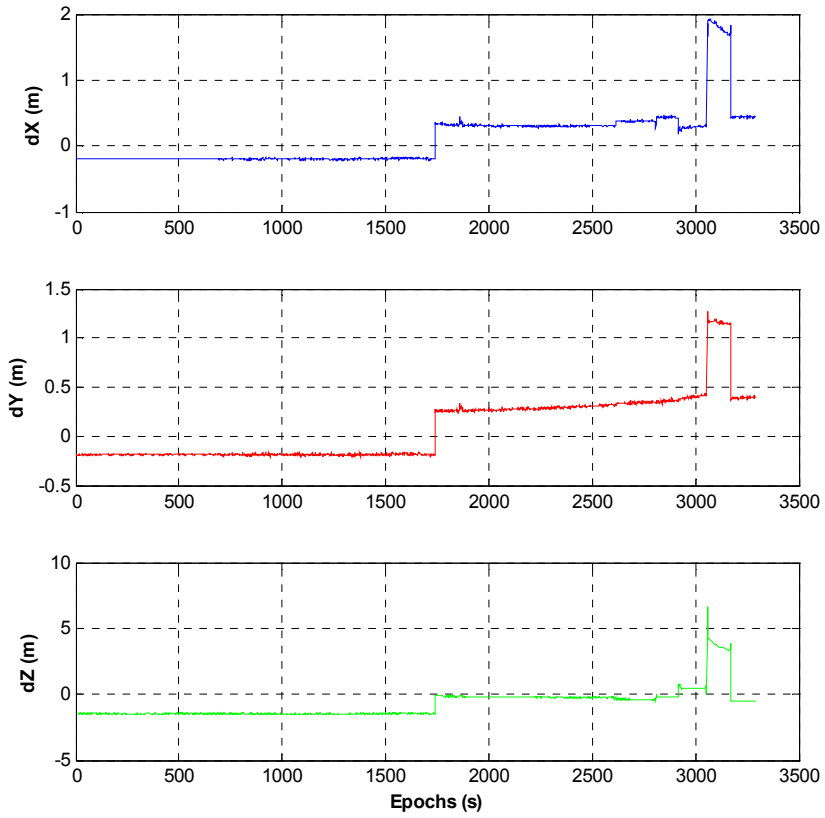

Figure 7.9 Differences in XYZ position components between the best satellites and reference data for the KJU27 session

The results from the multipath corrected file and the elimination of satellites highly contaminated with multipath, did not yield better results than the processing of the original file. The best estimates for the positions were obtained for the original file in the decimetre range for all the components. No improvements were generated when applying wavelet to the original file. The effects of multipath are more transparent in the wavelet data through the jumps. These jumps are known as cycle slips and cause an offset in the ambiguities which directly affects the code minus carrier equation. In this case, using wavelet analysis to separate multipath and noise is no longer effective. In all, the worst results were obtained when satellites severely contaminated with multipath were removed.

- **Session KSEP9**

TTC was used to process the GPS data collected on September 9th, 2009. The equipment set-up is described in Section 5.3. The initial 60-minute static data were split into 30, 20 and 10 minute static sessions; therefore, producing four sets of kinematic data with different initialization time. These different sets were compared to examine the effect of ambiguity resolution on the position estimates, Tables 7.10 to 7.13. For each data set, wavelet analysis was applied using the db8 (level 9) wavelet resulting in essentially multipath corrected files. Also, wavelet analysis was used to identify satellites highly contaminated with multipath. All the data were processed using TTC. The position results were compared to the reference data obtained from the Trimble R7 dual-frequency receiver and graphed (see Figures 7.10 to 7.12).

Table 7.10 Statistical information for the differences in XYZ position components between the original data and reference data for the KSEP9 session

	MEAN (mm)	STD (mm)	MAX (mm)	MIN (mm)
dX	-0.790	3.224	25.079	-23.840
dY	-0.653	3.076	25.912	-25.567
dZ	-3.617	8.321	59.871	-66.963

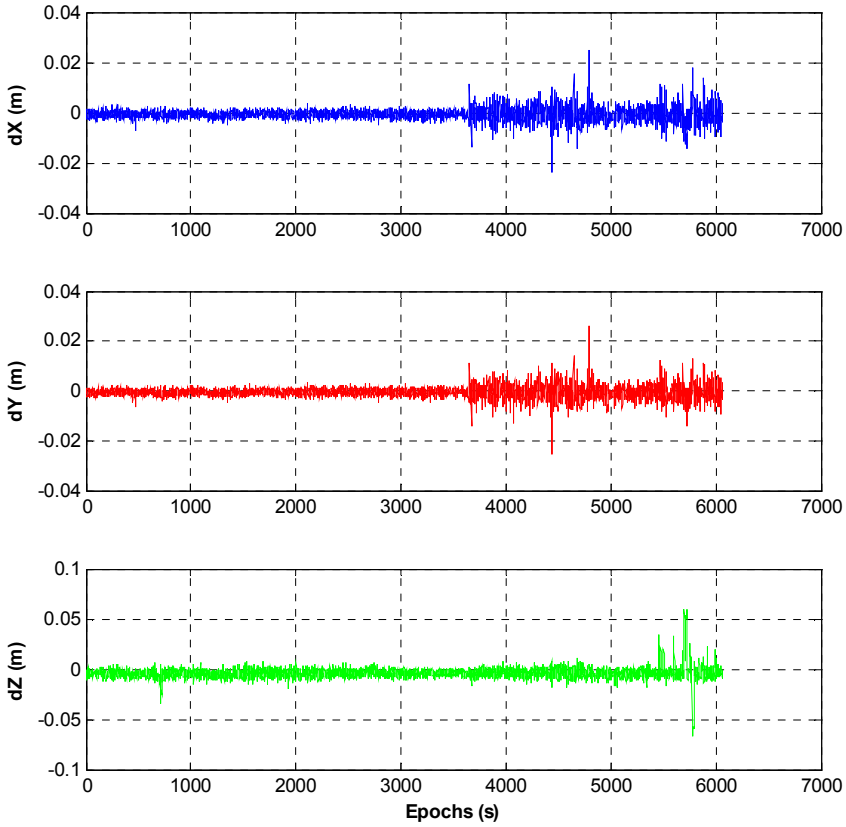

Figure 7.10 Differences in XYZ position components between the original data and reference data for the KSEP9 session

Table 7.11 Statistical information for the differences in XYZ position components between the multipath corrected data and the original data for the KSEP9 session

	MEAN (mm)	STD (mm)	MAX (mm)	MIN (mm)
dX	-0.793	3.224	25.079	-23.840
dY	-0.657	3.076	25.912	-25.567
dZ	-3.613	8.320	59.871	-66.963

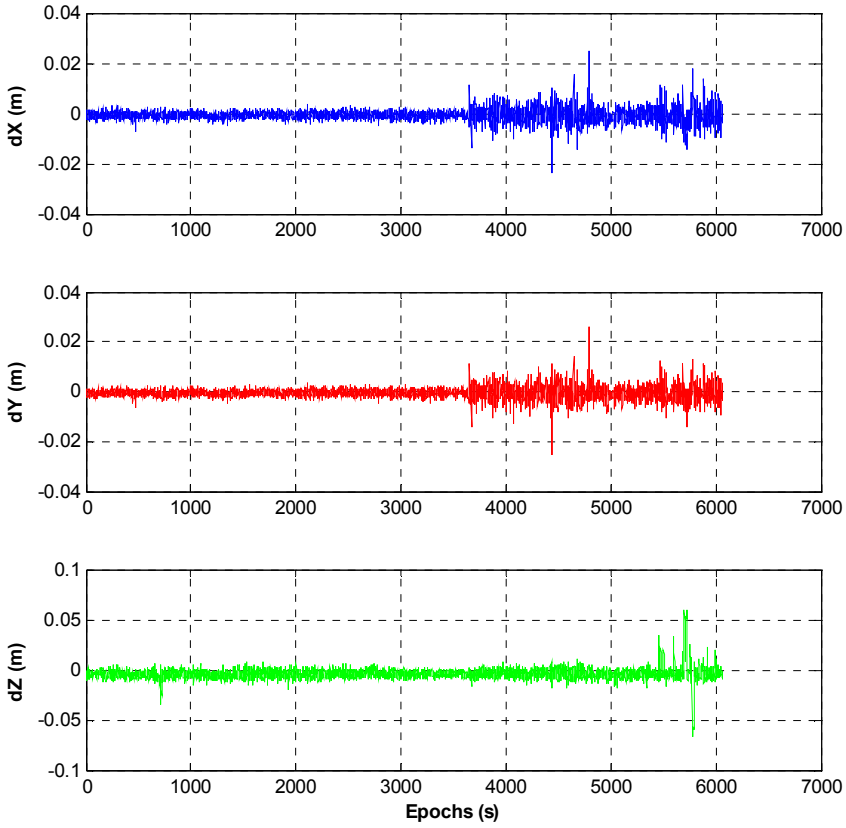

Figure 7.11 Differences in XYZ position components between the multipath corrected data and reference data for the KSEP9 session

Table 7.12 Statistical information for the differences in XYZ position components between the best satellites data and the original data for the KSEP9 session

	MEAN (mm)	STD (mm)	MAX (mm)	MIN (mm)
dX	-1.068	3.514	24.556	-22.653
dY	-1.190	4.092	25.132	-22.756
dZ	-2.201	16.412	111.010	-73.185

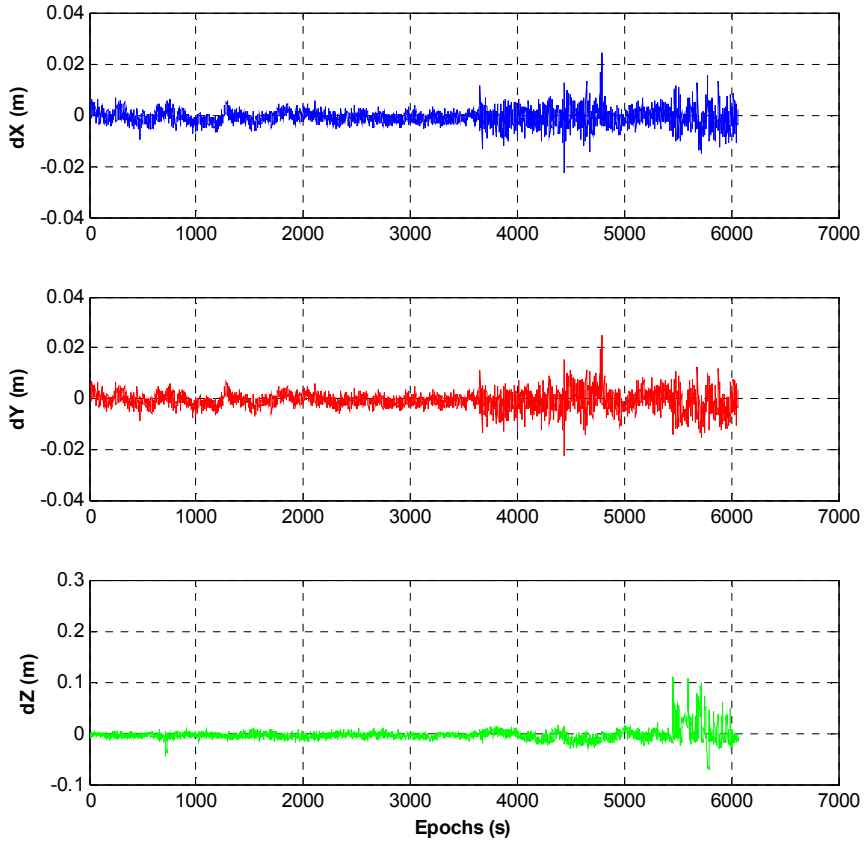

Figure 7.12 Differences in XYZ position components between the best satellites data and reference data for the KSEP9 session

Table 7.13 Statistical information for the differences in the XYZ position components for different static initialization intervals pertaining to the original (Original), multipath corrected (db8 L9) and best satellites (Best) files

Static Session (min)	Type	STD (mm)		
		dX	dY	dZ
60	Original	3.115	2.974	8.030
	db8 L9	3.115	2.974	8.030
	Best	3.403	3.963	15.823
30	Original	3.115	2.974	8.030
	db8 L9	3.115	2.974	8.030
	Best	3.403	3.962	15.823
20	Original	3.224	3.076	8.320
	db8 L9	3.224	3.076	8.320
	Best	3.515	4.092	16.413
10	Original	3.223	3.075	8.320
	db8 L9	3.224	3.076	8.320
	Best	3.515	4.092	16.412

Similar to the KJU27 results, none of the wavelet analysis techniques demonstrated a better solution based on standard deviations. Again, the poorest solution was obtained when satellites with a high level of multipath were removed. The results from the multipath corrected file produced better results than the original file.

The effects of different static intervals for initialization were also evaluated. Estimates for positions with initialization of 60 and 30 minutes displayed no changes in the standard deviations of each component. Minute differences were observed for the kinematic data when the

initialization time was reduced to 20 and 10 minutes; this can be attributed to the application of the OTF ambiguity resolution technique.

OTF is the most modern technique for carrier phase positioning where centimetre-level accuracy is required. This method does not require any static initialization and can commence without any time delay. A minimum of five satellites need to be tracked with a time interval of ten seconds to one minute without loss of lock in order to determine the integer ambiguity for dual-frequency data. Single-frequency data requires at least interval of about five to ten minutes (Trimble, 2007).

Overall, the differences are quite small, and therefore an initialization time of 10 minutes should generally be used. Further information regarding the static initialization times for 30, 20 and 10 minutes can be found in the Appendix.

8. Summary, Conclusions and Recommendations

8.1 Summary

The main objective of this research was to investigate the suitability of a low-cost GPS system for precise positioning in multipath environments. Wavelet analysis was utilized to extract approximations of multipath. Satellites strongly influenced by the multipath error were identified. In one approach, multipath-contaminated satellites were removed prior to processing the GPS data. Another approach, which was also examined, removed the code multipath error using the corresponding wavelet-based multipath estimates. Once the code multipath was essentially removed from the original measurements, the data processing was carried out.

Several static and kinematic data sets were collected in different types of environments. The code minus carrier combination of the GPS observables was employed. After accounting for certain errors, the remaining terms were essentially double the ionospheric delay, the ambiguity, multipath and noise. NOAA-based TEC values were implemented to account for the delay induced by the ionosphere. Next, the ambiguity term was removed by subtracting the mean of the residuals. At this stage all that essentially remained was low-frequency multipath and high-frequency noise.

Wavelet analysis was applied to separate the low- and high-frequency components. Different mother wavelets and decomposition levels were compared from the popular Daubechies family of wavelets. Db6 (level 7) and db8 (level 9) were the mother wavelets and decomposition levels selected for the static and kinematic modes, respectively, to isolate the multipath error. Standard deviations were calculated for the approximated multipath values for

each satellite. Those satellites severely contaminated with multipath were identified and removed. Another approach was also investigated where approximated multipath values were subtracted from the code measurements. Position estimates were obtained using the TTC and Bernese GPS software.

8.2 Conclusions

In this research, methods for enhancing the positional accuracy of low-cost GPS systems are described and evaluated for various sets of data collected in static and kinematic modes. Two methods are assessed; one method is based on the identification and removal of severely contaminated satellites and the other method involves the subtraction of approximated multipath values from the corresponding code measurements. The following conclusions were drawn from the experimental work conducted in this research for the static and kinematic data.

Static

Eliminating multipath-contaminated satellites proved to be the most effective. Significant improvements in position were consistently obtained for all three static stations when compared to the original data and the modified code measurements. Improvements of up to 86% in the RMSE were observed by this method when compared to the original data. Subtracting the approximated multipath from the code observable did improve the position estimates as well. The largest improvement for this method was achieved for the JU3A station where the RMSE was ameliorated by 39% when this method was compared to the original data. The other two

static sessions showed minor improvements in position. Overall, subtracting the wavelet-based multipath approximation from the code measurements proved to be an effective tool at generating the best position estimates.

Kinematic

Both methods did not show any improvement when compared to the original data. Extracting multipath estimates using wavelet analysis for the kinematic data did not demonstrate any amelioration. Cycle slips were abundantly present throughout the data series. This is caused by a loss-of-lock on satellites resulting in a discontinuity of the integer number of cycles in the carrier phase measurements, which in turn immensely influences the code minus carrier combination. Due to the cycle slips, the ambiguity term can no longer effectively be removed by subtracting the mean of the residuals. As a result, applying wavelet analysis to separate the multipath and noise is no longer affective. In general, the positional accuracy in the vertical component was affected the most when compared to the horizontal components. This is due mainly to satellite geometry and mask angle. The worst results were obtained by the removal of satellites severely contaminated with multipath. Kinematic data processing generally has lower redundant measurements in comparison with static data. Therefore, in general, one should abstain from removing satellites unless confident that a better solution can be realized.

8.3 Recommended Future Research

From the results achieved, various topics need to be further investigated in future research, including:

- Further probe the selection of an appropriate mother wavelet and level for multipath detection;
- Explore the use of other types of antennas;
- Model the other GPS errors to further increase positional accuracies;
- Investigate the multipath effects of other types of reflecting surfaces;
- Evaluate other types of receivers, as the Ashtech AC12 single-frequency receiver was only used; and
- Investigate the implementation of wavelet analysis with cycle-slip correction techniques especially for kinematic data.

REFERENCES

Al-Naqbi, A. (2008) “High accuracy positioning with low-cost single-frequency GPS system in multipath environments”. MASc. Thesis, Ryerson University, Toronto, Ontario, Canada, 158pp.

Alkan, R. M. and M. H. Saka (2007) “Centimeter level positioning with OEM-type GPS receivers”. Proceeding of the International Symposium on Modern Technologies, Education and Professional Practice in Geodesy and Related fields in Sofia, Bulgaria.

Anderson, D. and T. Fuller-Rowell (1999) “Space Environment Topics”. URL : http://sec.noaa,gov. Retrieved on July 25, 2009.

Aram, M., A. El-Rabbany, and S. Krishnan (2007) “Single frequency Multipath Mitigation Based on Wavelet Analysis”. The Journal of Navigation. Vol. 60. No. 2. pp. 281-290.

ATEC (2009) URL: http://www.atec.es/sensores.htm. Retrieved on August 30, 2009.

Beran, T., D. Kim, and R.B. Langley (2003). “Highprecision single-frequency GPS point positioning”. Proceedings of ION GPS 2003, Portland, Oregon,September 9-12.

Braash, M.S. (1996) “Multipath effects”. Global Positioning System: Theory and Application, Vol. 1, edited by B.W. Parkinson and J.J. Spilker, American Institute of Aeronautics and Astronautics, Washington D.C.

Dammalage, T. L., C. Satirapod, and S. Kibe (2008) “Wavelet transform application to C/A code multipath mitigation at GPS reference stations for improved differential GPS corrections”. Proceeding of the Symposium on GPS/GNSS in Tokyo, Japan.

Daubechies, I. (1992) “Ten Lectures on Wavelets”. Society for Industrial and Applied Mathematics (SIAM), Philadelphia, Pennsylvania.

El-Gizawy, M. (2003) "Development of an Ionosphere Monitoring Technique Using GPS Measurements for High Latitude GPS Users". Graduate Thesis, University of Calgary, Calgary, Alberta, Canada.

Elhabiby, M. (2007) "Wavelet Representation of Geodetic Operators". Ph.D. Thesis, UCGE No. 20250, Department of Geomatics Engineering, The University of Calgary, Calgary, Alberta, Canada, January, 148 pp.

El-Rabbany, A. (2006) "Introduction to GPS". 2nd Edition. Artech House Inc., Norwood, Massachusetts.

El-Sheimy, N., A. Osman, S. Nassar, and A. Noureldin (2003) ''Wavelet Multiresolution Analysis'', GPS World.

Estey, L., and C. Meertens (1999) "TEQC: The Multi-Purpose Toolkit for GPS/GLONASS Data". GPS Solutions. Vol. 3, No. 1, pp. 42-49.

Fu, W., and C. Rizos (1997) "The applications of wavelets to GPS signal processing". Proceeding of the 10th Int. Tech. Meeting of the Satellite Division of the U.S. Inst. of Navigation, Kansas City, Missouri, 16-19 September, pp. 1385-1388.

Fugal, Lee (2008) "Conceptual Wavelets in Digital Signal Processing". URL: http://www.conceptualwavelets.com/book.html.Retrieved on March 19th, 2008.

Goswami J. C. and A. K. Chan (1999) "Fundamentals of wavelets: Theory, algorithms, and applications". Wiley-Interscience, New York, USA.

Hofmann-Wellenhof, B., H. Lichtenegger and E. Wasle (2008) "GNSS Global Navigation Satellite System". Springer Wien, New York, USA.

IGS (2009) IGS Products, URL: http://igscb.jpl.nasa.gov/components/prods.html.

Keller W. (2004) "Wavelets in geodesy and geodynamics". Walter de Gruyter.

Komjathy, A. (1997) "Global Ionospheric Total Electron Content Mapping Using the Global Positioning System". Ph.D. dissertation, Department of Geodesy and Geomatics Engineering Technical Report No. 188, University of New Brunswick, Fredericton, New Brunswick Canada.

Kouba, J., and P. Héroux (2001) "GPS Precise Point Positioning Using IGS Orbit Products", GPS Solutions, Vol.5, No.2, pp. 12-28.

Kunysz, W. (2003) "A Three Dimensional Choke Ring Ground Plane Antenna". Proceedings of ION, September 2003.

Lachapelle, G. and M. Petovello (2006) "New GNSS Frequencies, Advantages of M-Code, and the Benefits of a Solitary Galileo Satellite". GNSS Solutions, May/June 2006, pp. 22- 27.

Langley, R. (2009) "GPS Constellation Maxed Out at 30". GPS World, November 2009, pp. 8-10.

Leid, A. (2004). "GPS Satellite Surveying". 3rd edition, Hoboken, NJ: John Wiley.

Liao, X. (2000) "Carrier Phase Based Ionosphere Recovery Over A Regional Area GPS Network". Graduate Thesis, University of Calgary, Calgary, Alberta, Canada.

Liu, Z., S. Skone, Y. Gao and A. Komjathy (2005) "Ionospheric modeling using GPS data". GPS Solutions, Vol. 9, pp. 63-66.

Mallat, S. (1998) "A wavelet tour of signal processing". Academic Press, New York, USA.

MATLAB (2009) URL. http://www.mathworks.com/products/matlab. Retrieved August 2009

Mendes, V. B. (1999) "Modeling the neutral-atmosphere propagation delay in radiometric space techniques". Ph.D. dissertation, Department of Geodesy and Geomatics Engineering Technical Report No. 199, University of New Brunswick, Fredericton, New Brunswick, Canada.

Mendizabal, J., R. Berenguer and J. Meléndez (2009) "GPS and Galileo: Dual RF Front-End Receiver, Design, Fabrication and Test". McGraw-Hill, New York, USA.

Mertins, A. (1999) "Signal Analysis: Wavelets, Filter Banks, Time-Frequency Transforms and Applications". Baffin Lane, Chichester: John Wiley & Sons Ltd.

Misra, P. and P. Enge (2002) "Global Position System Signals, Measurements, and Performances". Ganga-Jamuna Press.

NOAA (2009) "US Total Electron Content (US-TEC) User Documententation". URL: http://www.sec.noaa.gov/ustec/docs/Doc.pdf /. Retrieved on March 29th, 2009.

Ovstedal, O. (2002) "Absolute Positioning with Single Frequency GPS Receivers". GPS Solutions, Vol. 5, No. 4, pp. 33-44.

Park, K.D., R.S. Nerem, M.S. Schenewerk, and J.L. Davis (2004) "Site specific multipath characteristics of global IGS and CORS GPS sites". Journal of Geodesy, Vol. 77, pp. 799–803.

Satirapod, C. and C. Rizos (2001) "An approach to GPS analysis incorporation wavelet decomposition". Artificial Satellites, Vol. 36, No. 2, pp. 27-35.

Satirapod, C. and C. Rizos (2005) "Multipath mitigation by wavelet analysis for GPS base station applications". Survey Review, Vol. 38, pp. 2-10.

Schaer, S., W. Gurtner, and J. Feltens (1998) "IONEX: The IONosphere Map EXchange Format Version 1". Proceedings of the 1998 IGS Analysis Centers Workshop, ESOC, Darmstadt, Germany, February 9-11, 1998.

Seeber, G. (2003) "Satellite Geodesy", 2nd edition, Walter de Gruyter.

Sickle, J. (2008) "GPS for Land Surveyors". Taylor and Francis Group.

Souza, E.M., and J.F.G. Monico (2004) “Wavelet shrinkage: High frequency multipath reduction from GPS relative positioning.” GPS Solutions. Vol. 8, No. 3, pp. 152–159.

Spilker, J.J. and B. Parkinson (1996) “Overview of GPS operation and design”. Global Positioning System: Theory and Applications, Vol. 1, edited by B.W. Parkinson and J.J. Spilker, American Institute of Aeronautics and Astronautics, Washington D.C.

Teunissen, P.J.G. and A. Keusberg (1998) “GPS for Geodesy”. 2nd Edition, Springer-Verlag, New York, USA.

The MathWorks, INC. (2009) “Wavelet Toolbox”. URL: http://www.mathworks.com/. Retrieved on April 5th, 2009.

Trimble (2009) "Trimble Total Control User Manual.pdf". URL: http://www.trimble.com/. Retrieved on August 20th, 2009.

UNAVCO (2009) URL: http://facility.unavco.org/software/software.html. Retrieved on September 21, 2009.

Xu, G. (2007) “GPS Theory, Algorithms and Applications”. Springer, Berlin.

Zhong, P., X. L. Ding, D. W. Zheng, W. Chen and D. F. Huang (2008) “Adaptive wavelet transform based on cross-validation method and its application to GPS multipath mitigation”. GPS Solutions. Vol. 12, No. 2. pp. 109-117.

APPENDIX: SUPPLEMENTARY RESULTS

Daubechies mother wavelet and level determination

Table A.1 RMSE for the top ten Daubechies mother wavelets (db) and levels (L) for the MAY6, JU3A and JU3B static trials

MAY6	
Wavelet	**RMSE (m)**
db6 L7	0.023
db7 L6	0.024
db9 L7	0.024
db5 L7	0.024
db4 L6	0.025
db8 L6	0.025
db4 L5	0.026
db7 L5	0.026
db8 L5	0.026
db5 L5	0.026
db6 L5	0.026
db9 L5	0.026
db5 L6	0.026
db6 L6	0.026
db9 L6	0.026
db7 L7	0.028
db8 L7	0.029
db4 L7	0.030
db9 L8	0.040
db5 L8	0.040
db4 L8	0.043
db6 L8	0.044
db8 L8	0.046
db7 L8	0.047
db8 L9	0.048
db7 L9	0.049
db4 L9	0.049

JU3A	
Wavelet	**RMSE (m)**
db4 L8	0.008
db7 L7	0.010
db7 L8	0.011
db5 L8	0.013
db4 L7	0.014
db6 L7	0.015
db8 L8	0.015
db9 L8	0.017
db8 L7	0.018
db6 L8	0.020
db8 L9	0.020
db4 L6	0.022
db7 L6	0.023
db6 L6	0.023
db7 L9	0.023
db4 L5	0.025
db5 L7	0.026
db5 L5	0.026
db6 L5	0.026
db7 L5	0.027
db8 L5	0.027
db5 L6	0.027
db8 L6	0.027
db9 L7	0.027
db9 L5	0.028
db9 L6	0.029
db9 L9	0.030

JU3B	
Wavelet	**RMSE (m)**
db6 L8	0.016
db5 L8	0.018
db7 L7	0.018
db9 L8	0.019
db4 L7	0.019
db6 L7	0.020
db7 L8	0.021
db8 L5	0.021
db4 L8	0.021
db7 L6	0.021
db5 L5	0.021
db8 L7	0.022
db4 L5	0.022
db6 L6	0.022
db7 L5	0.023
db9 L5	0.023
db8 L8	0.023
db5 L7	0.024
db9 L7	0.024
db5 L9	0.024
db6 L5	0.024
db8 L9	0.025
db4 L9	0.026
db9 L9	0.026
db4 L6	0.026
db7 L9	0.026
db9 L6	0.028

db5 L9	0.051	db6 L9	0.049	db8 L6	0.028
db9 L9	0.052	db4 L9	0.059	db5 L6	0.029
db6 L9	0.053	db5 L9	0.061	db6 L9	0.029

Table A.2 Standard deviations for the top ten Daubechies mother wavelets (db) and levels (L) for the KM8A session

dX		dY		dZ	
Wavelet	**STD (m)**	**Wavelet**	**STD (m)**	**Wavelet**	**STD (m)**
db4 L9	0.108	db4 L9	0.106	db4 L9	0.437
db8 L9	0.122	db8 L9	0.125	db9 L9	0.452
db5 L9	0.125	db9 L9	0.126	db5 L9	0.457
db9 L9	0.126	db5 L9	0.126	db8 L9	0.458
Db7 L9	0.130	db7 L9	0.135	db7 L9	0.472
db6 L9	0.149	db6 L9	0.150	db6 L8	0.473
db4 L8	0.149	db9 L8	0.152	db6 L9	0.479
db8 L8	0.153	db5 L8	0.154	db9 L8	0.488
db9 L8	0.153	db4 L8	0.154	db5 L8	0.490
db5 L8	0.156	db8 L8	0.158	db7 L8	0.490
db7 L8	0.164	db6 L8	0.162	db8 L8	0.502
db6 L8	0.166	db7 L8	0.165	db4 L8	0.503
db4 L7	0.186	db4 L7	0.185	db4 L7	0.506
db5 L7	0.193	db5 L7	0.195	db5 L7	0.509
db9 L7	0.206	db9 L7	0.210	db9 L7	0.532
db8 L7	0.222	db8 L7	0.222	db6 L7	0.535
db6 L7	0.240	db6 L7	0.237	db8 L7	0.543
db9 L6	0.250	db9 L6	0.250	db7 L7	0.557
db7 L7	0.256	db7 L7	0.251	db7 L6	0.587
db5 L6	0.259	db5 L6	0.261	db9 L6	0.589
db6 L6	0.266	db6 L6	0.265	db6 L6	0.596
db8 L6	0.270	db8 L6	0.268	db4 L6	0.600
db7 L6	0.274	db7 L6	0.270	db8 L6	0.601
db8 L5	0.276	db9 L5	0.276	db5 L6	0.606
db9 L5	0.277	db8 L5	0.276	db6 L5	0.614
db5 L5	0.278	db6 L5	0.276	db9 L5	0.616

db7 L5	0.278
db6 L5	0.278
db4 L5	0.284
db4 L6	0.289

db7 L5	0.277
db5 L5	0.277
db4 L5	0.282
db4 L6	0.284

db5 L5	0.617
db7 L5	0.621
db8 L5	0.623
db4 L5	0.626

Table A.3 Standard deviations for the top ten Daubechies mother wavelets (db) and levels (L) for the KM8B session

dX	
Wavelet	**STD (m)**
db7 L9	0.186
db6 L9	0.315
db8 L9	0.625
db4 L9	0.813
db9 L9	1.044
db5 L9	1.062
db9 L8	1.369
db4 L8	1.400
db5 L8	1.409
db8 L8	1.447
db5 L7	1.918
db9 L7	1.927
db4 L7	1.962
db8 L7	2.073
db7 L8	2.078
db6 L8	2.096
db6 L6	2.173
db6 L7	2.209
db7 L6	2.276
db9 L6	2.306
db6 L5	2.314
db5 L6	2.318
db7 L7	2.324
db9 L5	2.326

dY	
Wavelet	**STD (m)**
db7 L9	0.191
db6 L9	0.350
db8 L9	0.722
db4 L9	0.940
db9 L9	1.219
db5 L9	1.236
db9 L8	1.604
db4 L8	1.639
db5 L8	1.651
db8 L8	1.697
db5 L7	2.250
db9 L7	2.261
db4 L7	2.300
db8 L7	2.433
db7 L8	2.441
db6 L8	2.461
db6 L6	2.551
db6 L7	2.596
db7 L6	2.674
db9 L6	2.707
db6 L5	2.719
db5 L6	2.719
db7 L7	2.730
db9 L5	2.734

dZ	
Wavelet	**STD (m)**
db6 L9	0.605
db7 L9	0.680
db5 L9	0.701
db9 L9	0.722
db8 L9	0.744
db4 L9	0.783
db9 L8	0.790
db8 L8	0.801
db5 L8	0.810
db4 L8	0.813
db7 L8	0.934
db6 L8	0.955
db9 L7	0.958
db5 L7	0.961
db4 L7	0.970
db8 L7	0.988
db6 L7	1.001
db6 L6	1.024
db7 L7	1.025
db7 L6	1.043
db9 L6	1.055
db5 L6	1.066
db8 L5	1.078
db4 L6	1.079

db7 L5	2.331
db4 L5	2.335
db5 L5	2.339
db4 L6	2.354
db8 L5	2.354
db8 L6	2.419

db7 L5	2.736
db4 L5	2.741
db5 L5	2.749
db4 L6	2.764
db8 L5	2.764
db8 L6	2.841

db8 L6	1.080
db5 L5	1.081
db4 L5	1.082
db7 L5	1.085
db9 L5	1.088
db6 L5	1.091